SCIENTIFIC REPORTS
nature research

OPEN

# Pheno-seq – linking visual features and gene expression in 3D cell culture systems

Received: 13 February 2019
Accepted: 12 August 2019
Published online: 26 August 2019

Stephan M. Tirier[2,3,7], Jeongbin Park[1,3], Friedrich Preußer[2,3,4], Lisa Amrhein[5,6], Zuguang Gu[3,8], Simon Steiger[2,3], Jan-Philipp Mallm[2,7,8], Teresa Krieger[1,2,3], Marcel Waschow[2,3], Björn Eismann[2,3], Marta Gut[9,10], Ivo G. Gut[9,10], Karsten Rippe[2,7], Matthias Schlesner[3,11], Fabian Theis[5,6], Christiane Fuchs[5,6,12], Claudia R. Ball[13], Hanno Glimm[13,14], Roland Eils[1,2,3,8,15] & Christian Conrad[1,2,3,8]

**Patient-derived 3D cell culture systems are currently advancing cancer research since they potentiate the molecular analysis of tissue-like properties and drug response under well-defined conditions. However, our understanding of the relationship between the heterogeneity of morphological phenotypes and the underlying transcriptome is still limited. To address this issue, we here introduce "pheno-seq" to directly link visual features of 3D cell culture systems with profiling their transcriptome. As prototypic applications breast and colorectal cancer (CRC) spheroids were analyzed by pheno-seq. We identified characteristic gene expression signatures of epithelial-to-mesenchymal transition that are associated with invasive growth behavior of clonal breast cancer spheroids. Furthermore, we linked long-term proliferative capacity in a patient-derived model of CRC to a lowly abundant PROX1-positive cancer stem cell subtype. We anticipate that the ability to integrate transcriptome analysis and morphological patho-phenotypes of cancer cells will provide novel insight on the molecular origins of intratumor heterogeneity.**

Three-dimensional (3D) cell culture systems (e.g. spheroids[1], organoids[2]) are characterized by self-organizing multicellular structures that reflect critical physiologic features of tissue geometry, cellular interactions and disease[3]. Therefore, they provide a relevant context for *in-vitro* testing of single cell behavior. During maturation in 3D culture, single cells undergo several rounds of replication accompanied by morphological and functional changes that rely on underlying gene expression programs. Depending on the initial single cell state, the resulting visual spheroid/organoid phenotype(s) can be highly informative for heterogeneous cellular functions[4–6] as well as for classification of tumor subtypes and disease states[7,8].

In particular, individual cancer cells obtained from the same tumor sample and grown under the same conditions frequently exhibit strong differences in replicative potential[4], invasive behavior[9] and drug responses[10].

[1]Digital Health Center, Berlin Institute of Health (BIH)/Charité-Universitätsmedizin Berlin, Berlin, Germany. [2]Center for Quantitative Analysis of Molecular and Cellular Biosystems (BioQuant), University of Heidelberg, Heidelberg, Germany. [3]Division of Theoretical Bioinformatics, German Cancer Research Center (DKFZ), Heidelberg, Germany. [4]Present address: Max Delbrück Center for Molecular Medicine, Berlin Institute for Medical Systems Biology, Berlin, Germany. [5]Helmholtz Zentrum München - German Research Center for Environmental Health, Institute of Computational Biology, Munich, Neuherberg, Germany. [6]Department of Mathematics, Technische Universität München, Munich, Germany. [7]Present address: Division of Chromatin Networks, German Cancer Research Center (DKFZ), Heidelberg, Germany. [8]Heidelberg Center for Personalized Oncology, DKFZ-HIPO, DKFZ, Heidelberg, Germany. [9]CNAG-CRG, Centre for Genomic Regulation, Barcelona Institute of Science and Technology, Barcelona, Spain. [10]Universitat Pompeu Fabra, Barcelona, Spain. [11]Bioinformatics and Omics Data Analytics, German Cancer Research Center (DKFZ), Heidelberg, Germany. [12]Faculty of Business Administration and Economics, Bielefeld University, Bielefeld, Germany. [13]Department of Translational Oncology, NCT Dresden, University Hospital, Carl Gustav Carus, Technische Universität Dresden, Dresden and DKFZ, Heidelberg, Germany. [14]German Cancer Consortium, Heidelberg, Germany. [15]Health Data Science Unit, University Hospital Heidelberg, Heidelberg, Germany. Correspondence and requests for materials should be addressed to C.C. (email: christian.conrad@bihealth.de)

This may be attributed to genetic diversity and clonal evolution[11], epigenetic alterations[12], microenvironmental influences[13] or stochastic gene expression[14]. This phenomenon of 'intratumor heterogeneity' is emerging as an essential driver of tumorigenic progression, treatment resistance and relapse[15].

A deeper understanding of morphological heterogeneity between clonal spheroids or organoids derived from a single patient requires the parallel acquisition of system-wide gene expression information. On the one hand, technologies for single cell RNA-seq (scRNA-seq)[16,17] have greatly improved the analysis of intratumor heterogeneity by enabling the unbiased detection of transcript abundances in individual cells[18–20]. Notably, these approaches do not provide a direct link to visual cellular phenotypes since the available protocols involve dissociation of cells and loss of their multicellular context. On the other hand, several powerful methods combining imaging and sequencing have been developed lately that enable transcriptomic profiling *in-situ* at high cellular resolution[21–25]. However, these methods require histological preparation which complicates or even prevents combined image-based and transcriptional profiling of one intact clonal spheroid or organoid. In addition, state-of-the-art methods for spatial transcriptomics require highly complex experimental setups[23–25] which limits broader applicability.

A recent landmark study highlighted the importance of directly combining imaging and sequencing in 3D cell culture systems by dissecting morphological and functional heterogeneities from clonal intestinal organoids[6], but yet without directly matching image and transcriptional features from the same organoid.

To address the abovementioned issues, we here introduce 'pheno-seq' to dissect cellular heterogeneity in 3D cell culture systems by directly combining clonal cell culture, imaging and transcriptomic profiling without histological preparation. Pheno-seq represents a new transcriptome analysis strategy that complements existing bulk and scRNA-seq approaches and enables a direct match of image features and gene expression in single clonal spheroids. We developed an experimental and computational workflow for high-throughput pheno-seq, including automated dispensing and imaging of single spheroids in barcoded nanowells as well as an automated image processing pipeline. We demonstrate the utility of pheno-seq in dissecting both morphological and transcriptional heterogeneity for established and patient-derived 3D-models of breast and colon cancer, respectively.

## Results

**Pheno-seq directly links visual phenotypes and gene expression in 3D cell culture systems.** We established the pheno-seq method using the MCF10CA cell line, a transformed derivative of the MCF10 progression line[26]. MCF10 cell lines reflect morphological phenotypes of epithelial breast cancer, in which normal epithelial cells undergo a stepwise transformation from local hyperplasia to premalignant carcinoma *in-situ* and invasive carcinoma[27]. The non-neoplastic parental cell line MCF10A forms polarized acinar spheroids closely resembling the lobular structures of the mammary gland[28]. In contrast, MCF10CA[29] cells have invasive and metastatic properties in xenografts[30]. Similarly, clonal MCF10CA spheroids display heterogeneous morphologies reflecting characteristics of late stages of breast cancer carcinomas, including 'round' (*in-situ*) and 'aberrant' (invasive) phenotypes (Supplementary Fig. 1a,b). With this cellular system, the pheno-seq protocol was established that consists of the following steps: (i) *Isolation and functional analysis of spheroid phenotypes*, (ii) *Data acquisition*, and (iii) *Integrative analysis of morphological phenotypes and transcriptome*.

*Isolation and functional analysis of spheroid phenotypes*. We developed a protocol to isolate single spheroids from reconstituted basement membrane (Matrigel) without perturbing their phenotypic identity (see Methods). We functionally analyzed the observed morphological heterogeneity by reseeding and culturing cells from both phenotype classes independently ('round' and 'aberrant'). Quantitative image analysis revealed enriched morphology appearances for each reseeded phenotype class indicating for high cell state stability and efficient isolation of different phenotype classes (Supplementary Fig. 1c).

*Data acquisition*. Pheno-seq combines automated imaging and transcriptomic profiling of individual clonal spheroids in a single workflow. This was achieved by repurposing the nanowell-based iCELL8 single cell sequencing system[31] for the processing of spheroid samples of up to 150 µm in size. Key modifications for accurate spheroid image profiling and subsequent processing for RNA-seq included cellular fixation[32], altered chip setup, higher-resolution microscopy, an automated image-processing pipeline and an interactive webtool for analysis and selection of spheroids for sequencing (Supplementary Figs 2 and 3, Fig. 1a,b). RNA-seq was conducted with the standard iCELL8 protocol that includes reverse transcription and cDNA amplification in nanowells as well as pooled 3′-end sequencing library preparation. With this setup, MCF10CA pheno-seq profiles of 210 spheroids were acquired.

*Integrative analysis of morphological phenotypes and transcriptome*. We analyzed MCF10CA pheno-seq profiles (n = 210 spheroids) by testing annotated and *de-novo* identified gene sets for coordinated expression variability[33]. 2D t-SNE visualization of RNA-seq data revealed two distinct clusters of spheroids that also differed strongly in several morphological image features (Fig. 1c,d and Supplementary Fig. 4). In particular, the observed heterogeneity in 'circularity' (Fig. 1c,d) is of primary interest as it informs about the epithelial integrity of epithelial/round spheroid (high circularity values) and more transformed invasive/aberrant phenotypes (low circularity values). Thus, these results indicate that the major transcriptional heterogeneity between spheroids relates to observed differences in morphological characteristics.

**In depth analysis of MCF10CA pheno-seq data.** Pheno-seq provides a wealth of data. In dependence of the specific cellular systems different biological questions can be addressed. For the MCF10CA system, we further investigated the molecular changes accompanying the transition from epithelial to invasive behavior. In breast cancer cells, this generally involves a specific gene expression program described as 'epithelial-to-mesenchymal transition' (EMT)[34]. Similarly, the spheroid cluster with low circularity values ('aberrant' phenotype) is defined by expression of an EMT signature[35], including the major mesenchymal marker vimentin (VIM). In contrast, the cluster with highly circular spheroids ('round' phenotype) is characterized by high expression of KRT15, a

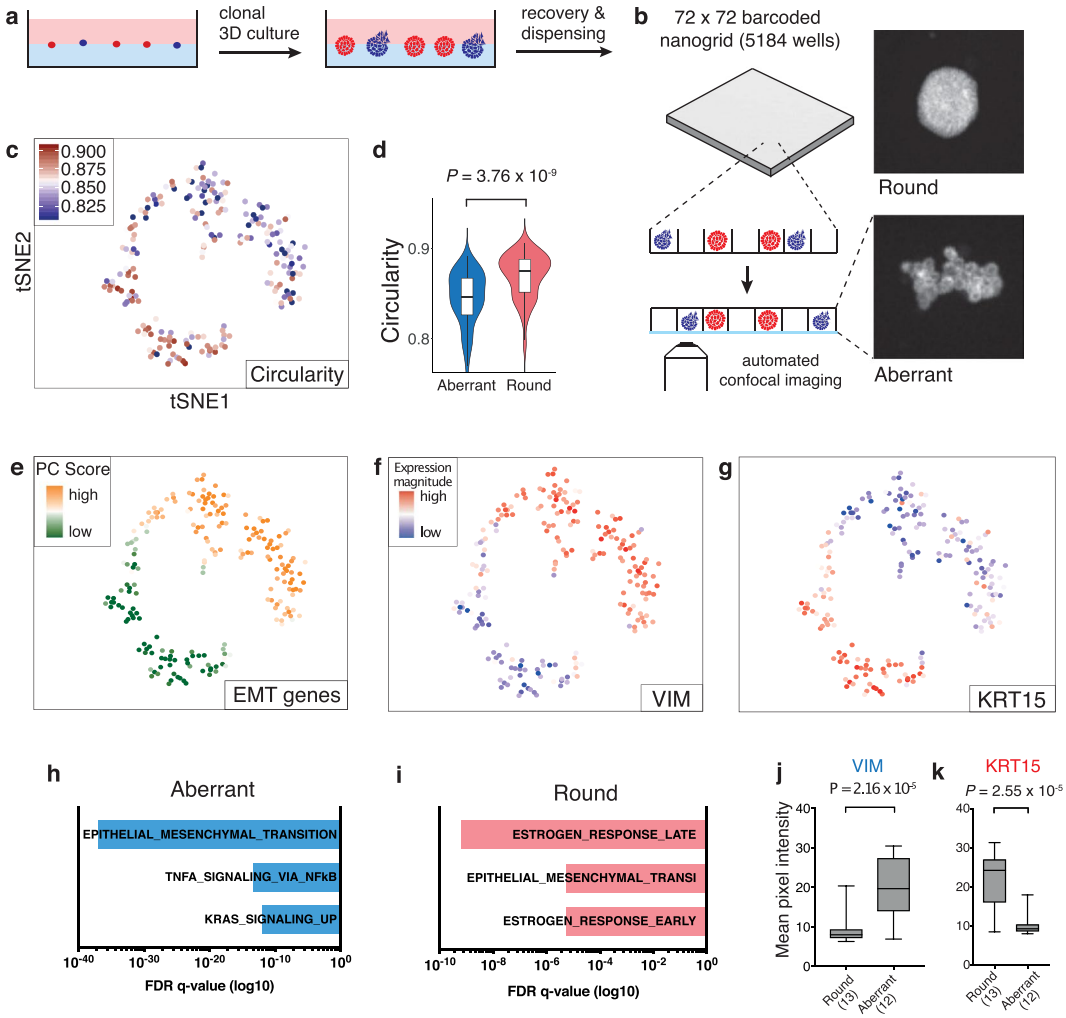


**Figure 1.** Pheno-seq directly links visual phenotypes and gene expression in 3D culture systems at high-throughput. (**a**) Workflow overview for the culture and recovery of clonal spheroids for inference of morphology-specific gene expression. (**b**) Pheno-seq workflow based on automated dispensing and confocal imaging of recovered spheroids stained by CellTrackerRed in barcoded nanowells. (**c**) 2D tSNE visualization of 210 pheno-seq 3′-end RNA-seq profiles with coloring based on image feature 'circularity'. For better visualization, all circularity values below 0.8 were set to minimum in the color code scheme. (**d**) Spheroid circularity plotted per cluster (k-means clustering, k = 2) as shown in (**c**). Violin-plot center-line: median; box limits: first and third quartile; whiskers: ±1.5 IQR. Indicated *P*-value from unpaired two-tailed Students t-test. (**e**) Same 2D tSNE visualization as shown in (**c**) with coloring based on PAGODA's PC scores for HALLMARK_EMT gene set derived from the Molecular Signature Database (MSigDB)[38]. (**f**,**g**) Same 2D tSNE visualization as shown in (**c**) with coloring based on expression magnitude for EMT marker VIM (**f**) and epithelial marker KRT15 (**g**). (**h**,**i**) Gene set enrichment analysis based on Hallmark gene sets[35] for 'aberrant' (**h**) and 'round' (**i**) phenotype specific genes identified by differential expression analysis[37] derived from the MSigDB. Bar plots show top three enriched gene sets ranked by FDR q-values. Example genes are VIM, TGFA, FAP for 'aberrant' and KRT15, CA2 and KRT16 for 'round' phenotypes. (**j**,**k**) Validation of phenotype-specific expression for VIM (aberrant) and KRT15 (round) by whole mount immunofluorescence (IF). Plotted values reflect mean pixel intensity per classified spheroid. Box plot center-line: median; box limits: first and third quartile; whiskers: min/max values. Numbers of samples indicated on x-axis under respective phenotype class. Indicated are *P*-values from unpaired two-tailed Students t-test.

basal-myoepithelial marker in the mammary gland[36] (Fig. 1e–g). Differential expression analysis[37] (fold change >1.3; adjusted p-value < 0.1) and gene set enrichment analysis[35,38] revealed concordant results. EMT related genes were highly enriched in aberrant spheroids, including VIM, JUN, RHOB, VCAN and FAP, respectively. Conversely, round phenotypes exhibit high expression of epithelial markers (e.g. KRT15, KRT16, KRT23 and DSG3) as well as genes involved in the response to the primary female sex hormone Estrogen (e.g. CA2, FABP5 and AGR2) (Fig. 1h,i). We validated spheroid phenotype-specific expression for VIM and KRT15 by quantitative immunofluorescence (Fig. 1j,k and Supplementary Fig. 5).

**Comparison of pheno-seq and scRNA-seq data.** Full-length pheno-seq (n = 8) and scRNA-seq (n = 166, reflecting approx. 6 spheroids) based on manually isolated spheroids yielded similar results with two distinct clusters that show a tight association of spheroids to their original phenotype class (Supplementary Fig. 6a–f). Notably, only pheno-seq enables a direct and quantitative association of image and transcriptomic features as standard scRNA-seq protocols requires multiple spheroids (>40 of each class) to achieve sufficiently high input material for cell capture.

Pheno-seq resulted in higher gene detection rates per sample compared to scRNA-seq, most likely due to the enhanced RNA-input that comprised a higher number of cells (Supplementary Fig. 6g, Supplementary Table 1). Surprisingly, we could not detect the major round-specific marker KRT15 by differential expression analysis of scRNA-seq data, even by generating synthetic pheno-seq profiles from averaged single-cell expression (Supplementary Fig. 7). This phenomenon could be due to the lower gene detection rate of scRNA-seq (Supplementary Fig. 6g) or due to the prolonged dissociation and processing procedure that can induce biases in detecting marker genes[39].

**Application of pheno-seq to a patient-derived colorectal cancer model.** We next set out to assess the functional association of visual phenotypes and gene expression in a clinically relevant and more complex 3D model of colorectal cancer (CRC)[4]. Dieter *et al*. identified and characterized functionally distinct subtypes of patient-derived CRC cells both *in vitro* and *in vivo* that differed in their long-term proliferative capacity[4]. The reported heterogeneity seems to be largely independent of mutational subclone diversity[40], indicating the presence of a differentiation-like hierarchy in CRC[41]. However, which lineage-related subtypes actually confer proliferative capacity has not been investigated, yet.

Single CRC cells form different spheroid phenotypes in terms of their replicative potential (Supplementary Fig. 8a). These include long-term proliferating, transient amplifying and postmitotic subtypes. In order to test whether spheroid forming capacity of single cells is associated with the proliferative capacity of their spheroid of origin, we reseeded cells derived from clonal spheroids that strongly differed in size after 10 days (20–40 µm vs. 70–100 µm). Quantitative image analysis revealed significant differences in spheroid forming capacity (Supplementary Fig. 8b), indicating that different sizes of clonal spheroids are associated with different compositions of functionally distinct subtypes. Moreover, reseeding of big spheroids resulted in mixed phenotypes (Supplementary Fig. 8a), in line with the hierarchical cancer stem cell model of CRC.

To identify transcriptional signatures that distinguish these heterogenous proliferative phenotypes, we performed pheno-seq based on clonal CRC spheroids cultured in a microwell setup (Fig. 2a, Supplementary Fig. 8c). Analysis of 95 HT-pheno-seq RNA-seq profiles and t-SNE visualization[33] confirmed two transcriptionally distinct clusters (Fig. 2b). Associated image analysis revealed a strong difference in spheroid size between both clusters (Fig. 2b,c).

**Assignment of lineage-related genes to heterogeneous CRC growth phenotypes.** We reasoned that the two different transcriptome types define spheroids that originated either from long-term proliferating ('big' phenotype) or transit-amplifying cells ('small phenotype'). Differential expression analysis[37] showed that the first cluster ('small'-phenotype) is enriched for secretory intestinal differentiation markers, including TFF3, KRT18 and SPINK4[42] (Fig. 2d). In contrast, the second cluster ('big'-phenotype) is characterized by the expression of genes previously described to be involved in intestinal stem/progenitor cell maintenance (e.g., CD44, MYC, NOTCH1, APP, MSI1 and ITGA6)[42,43], the formation of cell-cell junctions (e.g., EPCAM, CLDN4, CDH1) and WNT signaling (ZNRF3, LGR4, JUN). In addition, we identified several genes related to the γ-secretase machinery (e.g., NOTCH1, APP, ITM2B, APH1A and CD44) a key component of the Notch signaling pathway and target of novel therapies that aim to disrupt cancer stem cell signaling[44] (Fig. 2d). Finally, the pattern of this cluster-specific signature showed a high overlap with genes correlated with the major intestinal stem cell marker LGR5[41] (Fig. 2e). We could validate sphere size-dependent expression for selected lineage-specific markers by quantitative RNA-FISH (Fig. 2f, Supplementary Fig. 9).

Thus, pheno-seq is able to directly assign lineage-related genes to heterogeneous growth phenotypes. Furthermore, our results support the hypothesis of a hierarchical organization in CRC with a stem/progenitor-like cell population at the apex.

**Single-cell deconvolution of CRC pheno-seq data.** In order to increase the resolution of the pheno-seq transcriptome data and to computationally infer single-cell regulatory states we combined image analysis and gene expression deconvolution. First, cell numbers from CRC pheno-seq imaging were determined from the relationship of spheroid size and nuclei counts using light-sheet microscopy and 3D image analysis (Supplementary Fig. 10a). As the original pheno-seq data exhibited a poor association between library complexity and estimated cell numbers (Supplementary Fig. 10b), we downsampled the data to achieve a constant number of mRNA counts per estimated single cell content (Supplementary Fig. 10c). As expected, this approach introduced a positive correlation of cell numbers to housekeeping genes (e.g. ACTB) with a constant number of mRNA molecules per cell (Supplementary Fig. 10d). However, the heterogeneously expressed differentiation marker TFF3 does not exhibit any correlation with cell numbers, demonstrating the suitability of our normalization approach.

Next, we identified genes whose expression originates from heterogeneous single-cell regulatory states. A maximum likelihood inference approach initially developed to deconvolve cell-to-cell heterogeneities from random 10-cell samples[45] was used (Fig. 3a). Deconvolution of the entire CRC pheno-seq dataset revealed 1,012 genes that show an improved two-population fit compared to a one-population fit, assessed by the Bayesian information criterion (BIC) to calculate the quality of the fit relative to the number of inferred parameters (Fig. 3b). Gene set enrichment analysis revealed a high proportion of MYC targets as well as genes involved in the regulation of cell growth and proliferation (Fig. 3c). Strikingly, several identified genes are overlapping with

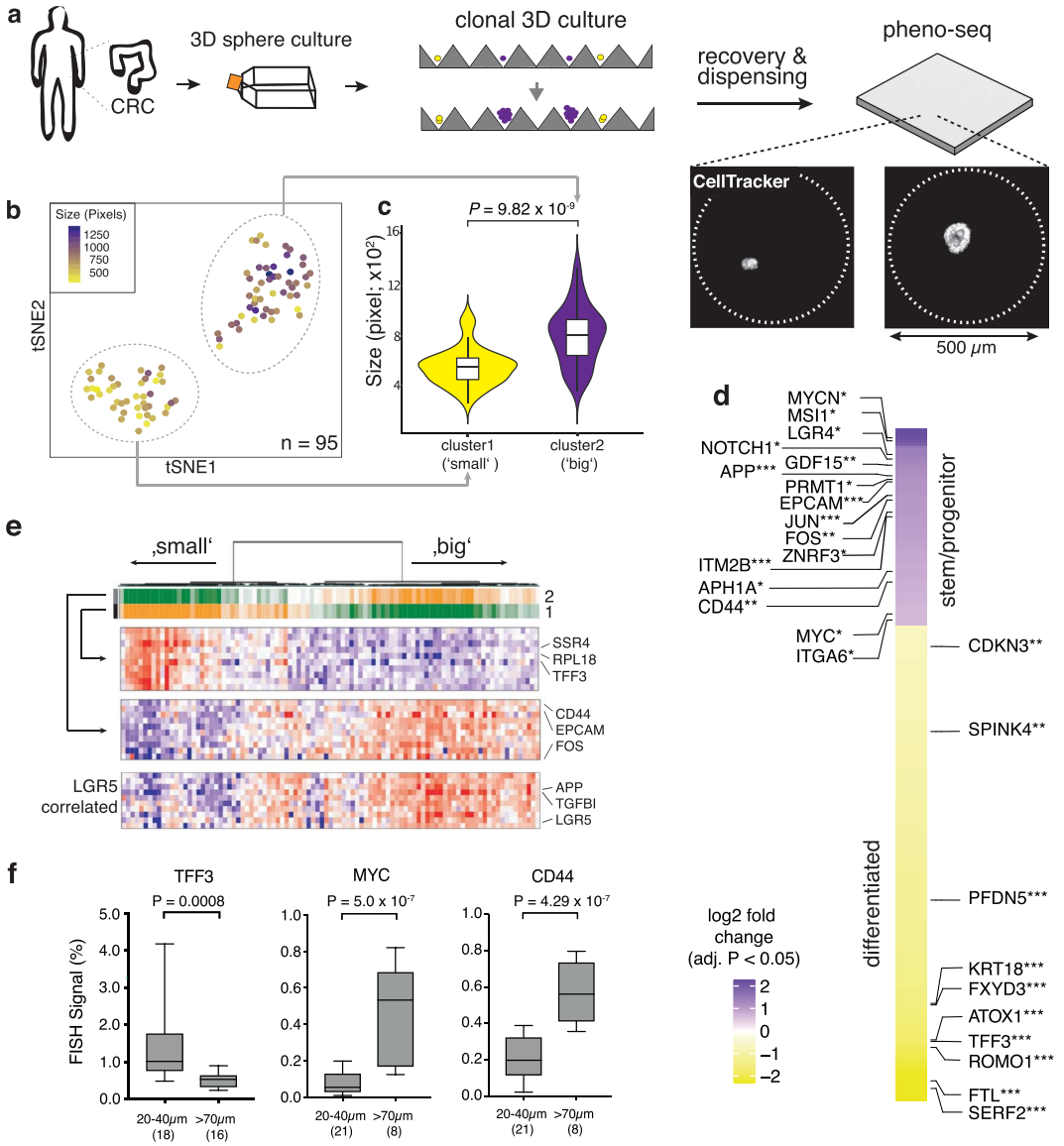


**Figure 2.** Pheno-seq with a 3D model of colorectal cancer links heterogeneous proliferative phenotypes to expression signatures enriched for lineage-specific markers. (**a**) Clonal 3D-culture in inverse pyramidal shaped microwells and recovery strategy for HT-pheno-seq of patient-derived CRC spheroids isolated from a liver metastasis. Yellow and purple indicate heterogeneous subpopulations with functional differences in proliferative capacity[4]. (**b**) 2D tSNE visualization of 95 HT-pheno-seq expression profiles. Coloring by sphere size (pixel). (**c**) Spheroid size plotted per cluster. Violin-plot center-line: median; box limits: first and third quartile; whiskers: ±1.5 IQR). Indicated *P*-value calculated from unpaired two-tailed Students t-test. (**d**) Heatmap reflecting differential expression analysis[37] of identified clusters in (**b**). Selected genes are listed beside the heatmap; Fold change >1.5; adjusted *P*-value < 0.05; *$P < 0.05$, **$P < 0.01$, ***$P < 0.001$; 'small' cluster1: 313 differentially expressed genes; 'big' cluster: 130 differentially expressed genes. (**e**) PAGODA RNA-seq analysis heatmap of CRC spheroid pheno-seq data. Dendrogram reflects overall clustering and the rows below represent top two significant aspects of heterogeneity based on HALLMARK/GO gene sets derived from the MSigDB[38] and on *de-novo* identified gene sets. High PC Scores correspond to high expression of associated gene sets. Expression patterns below reflect top 10 loading genes for selected gene sets that are associated with respective aspects. Bottom: Expression pattern of genes most highly correlated with intestinal stem cell marker LGR5 (Pearson's correlation). (**f**) Validation of pheno-seq by quantitative RNA-FISH for size-dependent differentiation marker TFF3 and cancer stem cell markers CD44/MYC. Plotted values reflect the pixel fraction that exceeds the background threshold per spheroid (Box plot center-line: median; box limits: first and third quartile; whiskers: min/max values; *P*-values from unpaired Students t-test. Numbers of samples n indicated on x-axis under respective class).

murine and human intestinal stem cell markers revealed by scRNA-seq[42,46], including SMOC2, RGMB, APP, MAPK1, EPHB3 and RNF43, respectively (Fig. 3d). Furthermore, we additionally identified the transcriptional regulator PROX1 whose expression is positively correlated with cell numbers and with expression of the major intestinal stem cell marker LGR5 (Fig. 3e). This finding was validated by RNA-FISH in CRC spheroids where a

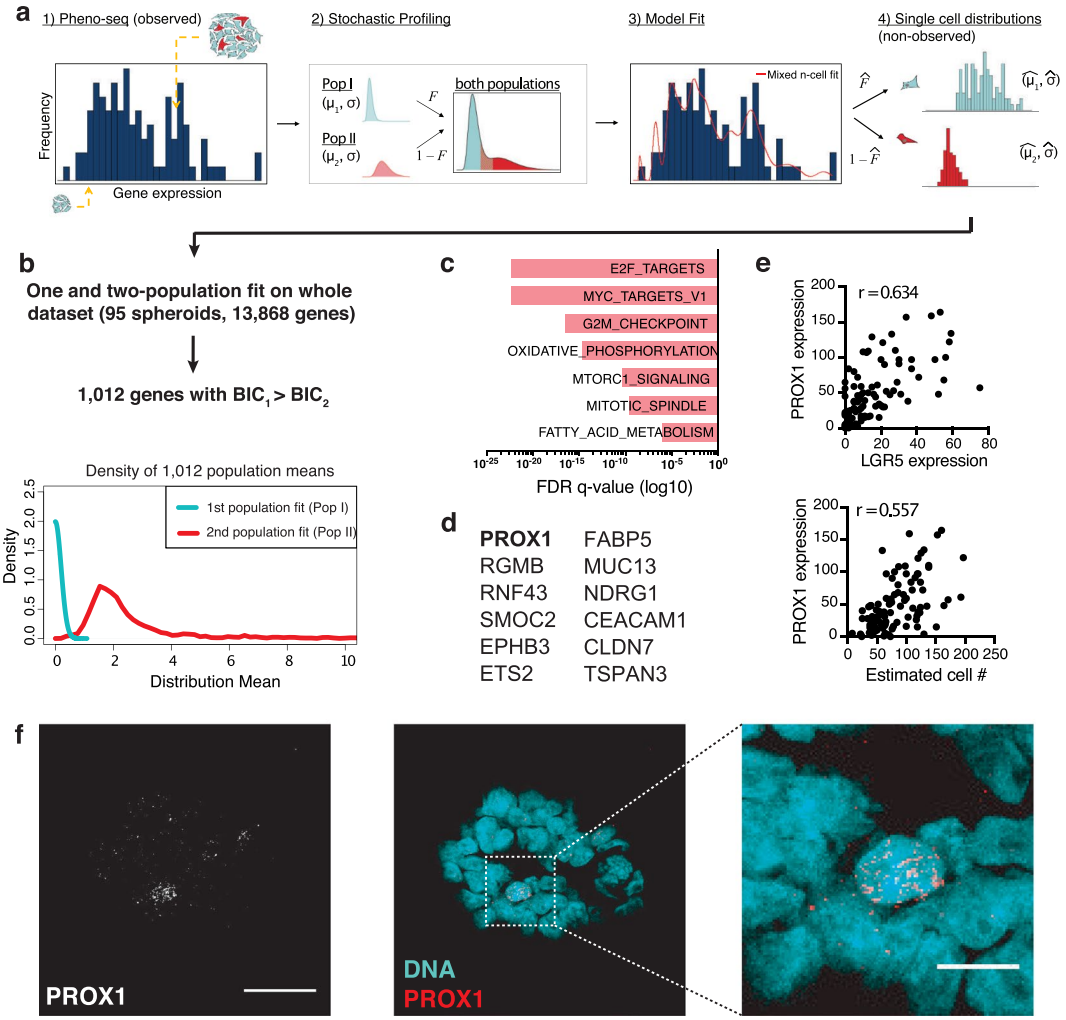


**Figure 3.** Single-cell deconvolution of CRC spheroid pheno-seq data by maximum likelihood inference. (**a**) Concept of adapted maximum likelihood approach[45] based on estimated cell numbers and transformed pheno-seq data (n = 95): (1) Acquired and transformed pheno-seq data based on estimated cell numbers build a distribution of measurements for inference by the model. Coloring of cells in spheroids: red = stem-like; cyan = differentiated. (2) Assumptions on single cell distributions: Model of heterogeneous gene regulation in which single cells are supposed to exhibit gene expression at low (Pop I) or high (Pop II) levels with a common coefficient of variation. The four parameters of the model are the log-mean expression for each subpopulation ($\mu_1$ and $\mu_2$), the proportion of cells in the high subpopulation ($F$), and the common log-SD of expression ($\sigma$). (3) Based on the model in step 2, a likelihood function is derived that takes different numbers of cells per spheroid into account. The likelihood function is then maximized by searching through the four parameters of the model to identify those that are most likely given the experimental observations. 4) These four parameters define the inferred single cell distributions of the low and high-level populations. (**b**) 1,012 genes show an improved two-population fit compared to a one population fit (BIC: Bayesian information criterion). Densities of the means of the first (Pop I: low regulatory state) and second population (Pop II: high regulatory state) for all identified 1,012 genes. (**c**) Gene set enrichment analysis for two-population genes based on Hallmark gene sets[35] derived from the MSigDB[38]. Bar plot showing top enriched gene sets ranked by FDR q-values. (**d**) Selected human colonic stem and differentiation markers[46] that have been identified by pheno-seq deconvolution. (**e**) Scatter plots for relations of PROX1 expression and estimated cell numbers (lower) and between PROX1 expression and expression of the major intestinal stem cell marker LGR5 (upper) as well as associated Pearson's correlation coefficients (r). (**f**) RNA-FISH staining of CRC spheroids for PROX1 (Atto550) and DAPI counterstaining for visualization of DNA. Merged images: DNA: cyan; PROX1: red. Images represent Z-projections (scale bar 30 µm and 10 µm for magnified merged image).

low-abundant PROX1$^+$ cell population was identified (Fig. 3f). We conclude that image analysis and deconvolution of pheno-seq data provides information about gene expression patterns at the single cell level even without acquiring additional single cell expression profiles.

**Linking proliferative capacity to a low-abundant stem cell subtype in CRC.** We next aimed to directly link specific intestinal lineage subtypes to their functional proliferative phenotype. Using markers

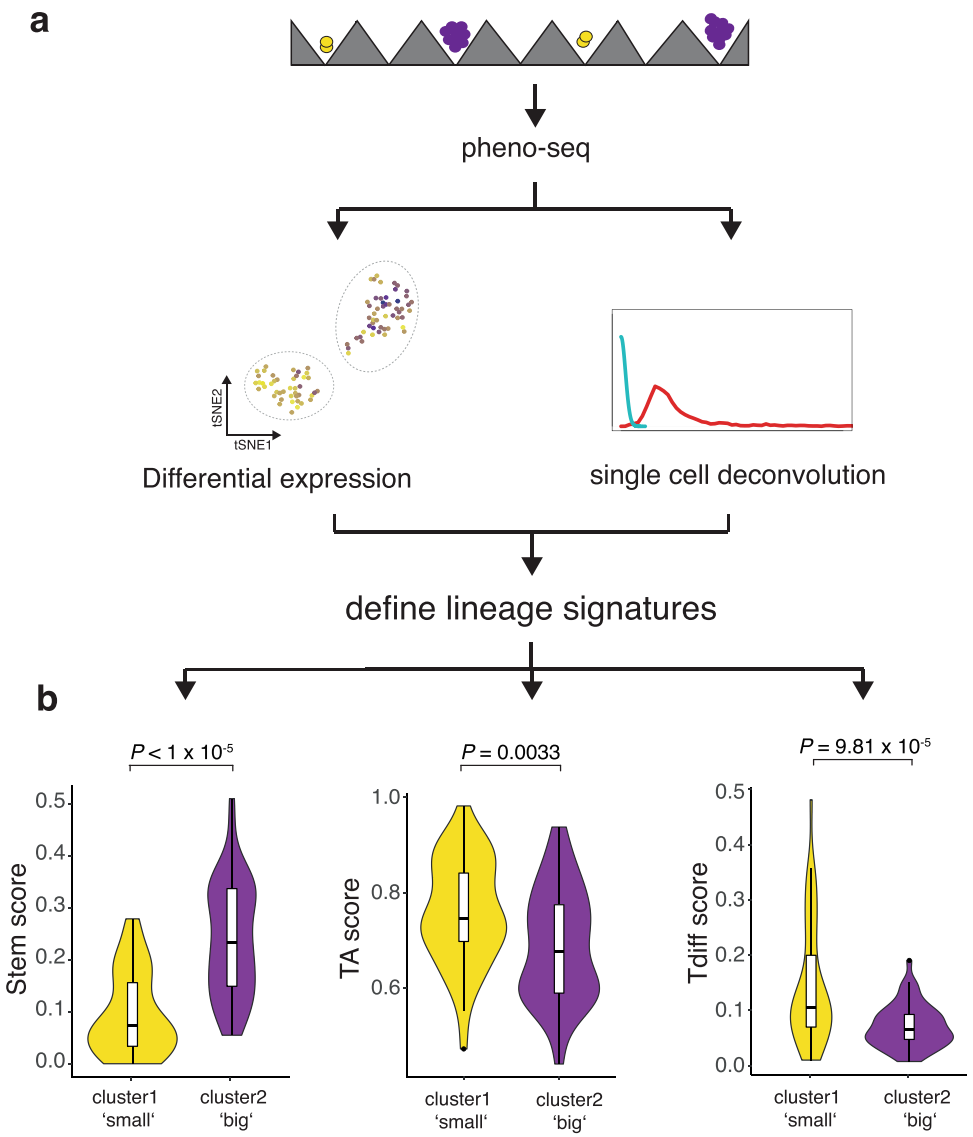


**Figure 4.** Scoring of pheno-seq data for subtype-specific signatures links long-term proliferative capacity to a stem-like subtype in CRC. (**a**) Strategy to define lineage-specific expression signatures. Stem: PROX1 correlated genes (top 20); Transit-amplifying (TA): Ribosomal genes (n = 24); Terminally differentiated (Tdiff): TFF3 correlated genes (top 20). (**b**) Violin Plots showing (cluster-specific) pheno-seq expression profiles scored for subtype signatures (see Methods). Violin-plot center-line: median; box limits: first and third quartile; whiskers: ±1.5 IQR). Indicated P-value calculated from unpaired two-tailed Students t-test.

obtained from both differential expression analysis and single cell deconvolution, we defined expression programs that are specifically associated with one of the three expected and functionally different stem (long-term proliferating), transit amplifying (TA) and terminally differentiated (Tdiff, postmitotic) subtypes[4] (Fig. 4a). We defined stem and Tdiff gene expression programs as the averaged expression of the (top 20) genes most highly correlated with PROX1 or TFF3, respectively. Grün *et al.* could link expression of ribosomal genes to a TA compartment in intestinal organoids[47]. In line with these observations, we identified a high number of ribosomal genes by pheno-seq deconvolution (GO_RIBOSOME, FDR q-value $3.53 \times 10^{-15}$). We therefore defined a ribosomal gene signature as TA expression program (n = 24 genes).

To approximate subtype abundances in individual spheroids, we scored pheno-seq expression profiles for stem, TA and Tdiff signatures and compared scores between detected pheno-seq clusters that are associated with functional differences in proliferative capacity. Notably, whereas the 'big'-phenotype cluster exhibited higher scores for the stem-signature, the 'small'-phenotype cluster showed higher scores for both TA and Tdiff-signatures (Fig. 4b). These results indicate that TA and Tdiff cells, but not stem-like cells, are highly abundant in spheroids with limited proliferative capacity and that a low-abundant stem-like subtype exclusively confers long-term proliferative capacity.

## Discussion

Patient-derived 3D cell culture systems are emerging as an important approach for clinical decision making[7]. Accordingly, there is increasing need to understand the heterogeneity of functional oncogenic phenotypes in cancer. Here, we introduce pheno-seq as a novel approach to directly combine imaging and next generation sequencing at high-throughput to explain clonal heterogeneity at the morphological and molecular level.

Our method represents a complementary approach to scRNA-seq of cell suspensions, which is currently the primary method to identify cellular subpopulations: (i) Pheno-seq directly and quantitatively links heterogeneous spheroid morphologies to underlying gene expression in a single experiment. (ii) No further histological preparations are required since 3D phenotypes of whole spheroids formed by living cells are evaluated. This is critical to cover the whole spectrum of transcripts that derive from one clonal spheroid. (iii) Pheno-seq reduces dissociation biases and enables a higher transcriptome coverage per sample due to the higher cell number input. This can be advantageous to identify marker genes that are missed by scRNA-seq. (iv) Using plates or a recent ICELL8 protocol[48], pheno-seq can be also used to analyze full-length RNA transcripts. Notably, plate-based approaches still require the manual isolation of spheroids which significantly reduces the throughput but might enable custom imaging protocols for higher resolution microscopy. (v) By integrating scRNA-seq data and applying deconvolution approaches, the resolution of the gene expression profiles can be increased to the single cell level.

As a proof-of-concept we established pheno-seq with the MCF10CA breast cancer model. We revealed epithelial and estrogen-responsive genes that define an *in-situ* like 'round' phenotype. Conversely, the expression of this signature decreases with more invasive (aberrant) growth behavior with simultaneous upregulation of EMT related genes.

Next, the utility of pheno-seq for analyzing functional cancer cell heterogeneity was demonstrated in a more complex model of CRC where the number of functionally distinct subtypes exceeds the number of observable phenotypes. Our results show that CRC spheroid cultures do not solely contain cancer stem cells (CSCs) but exhibit a surprisingly high degree of differentiation. In addition, the results strongly indicate that CRC 'sphere-assays' enable the measurement of self-renewing capacity of a distinct PROX1$^{+}$ CSC subtype and that more differentiated subtypes have limited potential to self-renew *in-vitro*[1]. Interestingly, PROX1 is normally expressed in the intestinal enteroendocrine lineage[49]. However, two studies based on mouse tumor models suggest a role for PROX1 in cancer stem cell maintenance and metastatic outgrowth[50,51].

We expect that the combination of functional single cell growth assay in 3D cultures with combined image and gene expression profiling will be widely applied in cancer biology, ranging from primary[8] to circulating tumor cells (CTCs)[52]. Furthermore, the application of pheno-seq is not restricted to cancer models but could be also a valuable approach to understand non-synchronized developmental processes[6]. We believe that pheno-seq becomes even more powerful with increasing resolution and content of imaging, employing enhanced 3D-image acquisition, integrated staining by IF or live-dyes, and time-lapse microscopy, respectively. Pheno-seq can also be easily extended to other low-input, next-generation sequencing modalities such as chromatin accessibility sequencing[53] or applied to pooled-screening approaches[54]. Thus, pheno-seq provides an additional perspective to study functional tumor cell heterogeneity in a variety of biological and clinical applications.

## Methods

**Breast cancer model MCF10CA.** *Cell culture.* For 2D cell culture, the cell line MCF10CA1d clone 1 (acquired from The Barbara Ann Karmanos Cancer Institute), a transformed derivative of the MCF10A 3D-culture model for acinar morphogenesis of the mammary gland, was routinely passaged in 25 $cm^2$ culture flasks. Cells were cultured in growth medium consisting of DMEM/F12 medium supplemented with 5% horse serum, 10 µg/ml Insulin, 20 ng/ml EGF, 0.5 mg/ml hydrocortisone and 100 ng/ml Cholera toxin. Cells were passaged at approximately 80% confluency with 0.05% Trypsin. The cell line was authenticated using a Multiplex human Cell line Authentication test (http://www.multiplexion.de/).

For 3D 'on top' assays, cells were cultured in assay medium (growth medium with only 2% horse serum and 5 ng/ml EGF) in 24-well cell culture plates. As a basement membrane surrogate, a bed of laminin-rich hydrogel (Matrigel®, Corning) was generated by adding 70 µm cold Matrigel into the center of pre-wetted wells. The Matrigel bed was then dried for 20 min at 37 °C. For single-cell seeding, 2D cultures were dissociated into single-cell suspensions, washed once in assay medium, passed through a 35 µm strainer and counted. Subsequently, 4000 cells were seeded per well in 400 µl assay medium with 5% Matrigel by adding cell suspensions in a 45° angle to the wall of the well, which resulted in uniform distribution of single-cells throughout the well. Medium was replaced every 3 days and cells cultured for up to 12 days. All scRNA-seq and pheno-seq experiments were carried out after 5 days in 3D-culture.

*Spheroid recovery from hydrogel.* After MCF10CA cells were cultured in 3D for 5 days, medium was removed from wells and 500 µl filtered and pre-warmed Dispase (Sigma) was added. The hydrogel-matrix was detached from wells by scratching over the well bottom with a 1000 µl pipette tip and the whole Dispase-Matrigel suspension was carefully resuspended five times. Afterwards, spheroids were incubated at 37 °C for 7 min. Spheroids were then transferred to a 15 ml falcon and 5 ml assay medium was added and resuspended slowly with a 5 ml pipette. Subsequently, spheroids were spun down (300 g, 3 min) and resuspended in DMEM. We do not recommend using PBS due to perturbation of spheroid morphology. In general, this procedure resulted in approximately 2000 isolated spheroids per well.

*Spheroid isolation and dissociation to single-cell suspensions.* In order to isolate and classify individual MCF10CA spheroids prior to dissociation, suspensions were diluted to 100 spheroids per ml in assay medium and distributed into GravityTRAP™ ultra-low attachment 96-well plates (PerkinElmer, 10 µl per well). Plates were centrifuged for 2 min at 250 g. The V-shaped wells with 1 mm diameter flat-bottom enabled efficient classification (round vs.

aberrant) of spheroids with 10x or 20x objectives of an inverted brightfield microscope. After 40 spheroids had been isolated and identified for each class (~30–45 min), 50 µl Accumax (Sigma) was added to each well followed by an incubation of 10 min at 37 °C. To stimulate dissociation, shear forces were applied by resuspending wells of one class with a 200 µl pipette without changing the tip. After a second incubation of 5 min at 37 °C, wells of one class were pooled in 1.5 ml microcentrifuge tubes, spun down at 300 g for 3 min and resuspended in either assay medium or DMEM/F12.

*Reseeding assay.* For independent reseeding of round and aberrant 3D phenotypes, 30–40 spheroids of one class were isolated, dissociated and pooled as described above. A 10 µl Matrigel bed was prepared during dissociation in 15 µ angiogenesis slides (Ibidi). After centrifugation, cells were resuspended in 50 µl assay medium (+5% Matrigel) and added to pre-treated angiogenesis slides. Medium was replaced every 3 days and cells were cultured for up to 6 days.

*MCF10CA single-cell capture, mRNA library preparation and sequencing.* For MCF10CA single-cell RNA sequencing experiments, spheroids were dissociated as described above and resuspended in DMEM/F12 medium. Capture, full-length cDNA synthesis and amplification was performed on the C1 Single-Cell Auto Prep system for mRNA Seq (Fluidigm) using the IFC for up to 96 cells (medium size 10–17 µm). Cells at a concentration of 350 cells/µl were mixed with C1 Cell Suspension Reagent (Fluidigm) at a ratio of 4:1 immediately before loading on the IFC. Single-cell capture was assessed with an inverted brightfield microscope. Workflow and reagents for single-cell RNA extraction, reverse transcription (RT) and mRNA amplification (18 cycles) were used as described in the SMARTer Ultra Low RNA Kit (for Fluidigm C1). Sequencing libraries were generated with the Nextera XT kit (Illumina) according to an adapted Fluidigm protocol. Concentration and quality of cDNA and sequencing libraries was assessed by a fluorometer (Qubit) and by electrophoresis (Agilent Bioanalyzer high sensitivity DNA chips). Libraries of up to 24 cells were pooled and sequenced as 1 × 50-bp reads on an Illumina HiSeq 2000 machine.

*Full length pheno-seq workflow, library preparation and sequencing.* For full-length pheno-seq, suspensions were diluted to 500 spheroids per ml in DMEM and 2 µl was carefully dispensed to the wall of the well of GravityTRAP™ 96-well plates followed by vertical tapping of the plate. Wells with single spheroids were then microscopically classified. For RNA extraction with the Arcturus PicoPure kit (ThermoFisher), 50 µl extraction buffer was directly added to 96-wells, incubated for 2 min at RT and then transferred to 1.5 ml LoBind microcentrifuge tubes (Eppendorf). RNA was isolated as described in the PicoPure Kit (Appendix B and Section 4B.2) including on-column DNase digestion (Appendix A, RNase-Free DNAse Set, Qiagen). RNA was eluted in Nuclease-free water (~10 µl) and used as input for full-length cDNA synthesis and amplification (16 cycles) by the SMART-Seq® v4 Ultra Low Input RNA Kit for sequencing (TakaraBio). Sequencing libraries were generated with the Nextera XT kit (Illumina) as described in the SMART-Seq® v4 protocol. Concentration and quality of cDNA and sequencing libraries was assessed by a fluorometer (Qubit) and by electrophoresis (Agilent Bioanalyzer high sensitivity DNA chips). Ten libraries were pooled and sequenced as 1 × 50-bp reads on an Illumina HiSeq 2000 machine.

*MCF10CA high-throughput pheno-seq workflow, library preparation and sequencing.* The following section describes the primary high-throughput pheno-seq workflow, including staining, cellular fixation, dispensing, cDNA amplification and NGS library preparation. For detailed description of microscopy and image analysis see section 'Microscopy and image analysis' and supplementary information.

For high-throughput (HT-)pheno-seq, we adapted and improved the nanowell-based Wafergen iCELL8 scRNA-seq system, that integrates imaging and gene expression profiling of big samples of up to 100 µm[55]. First, spheroids were stained 3 hours with 10 µM CellTracker™ Red CMTPX dye and 1 µg/ml Hoechst 33258 (ThermoFisher). Afterwards, spheroids of six wells were recovered as described above and washed once with 7 ml DMEM (Life Technologies). Only three wells were pooled per 15 ml falcon tube for centrifugation. The reversible cross-linker dithio-bis(succinimidyl propionate) (DSP) was prepared for cellular fixation as previously described[32] and directly filtered through a 10 µm strainer. Spheroids were resuspended in 400 µl DSP and incubated for 30 min at room temperature. After fixation, spheroids were washed two times with cold PBS (centrifugation at 650 g and 500 g, 3 min, 4 °C) and then resuspended in 650 µl cold PBS with 1x second diluent (for iCELL8) and 0.4 U/µl recombinant RNase Inhibitor (TakaraBio). Spheroids were dispensed into a barcoded 5184-nanowell chip with the iCELL8 Single-Cell System (TakaraBio) as described in the Rapid Development Protocol (in-chip RT-PCR amplification). As a control, we first dispensed, imaged and processed one chip without cellular fixation using the default settings, the standard microscope and the provided CellSelect™ software.

For improved HT-pheno-seq we applied the following modifications: Between the three dispensing intervals, wells in the 384-well source plate were stirred with a 200 µl pipette tip just before intake of suspensions with the dispensing heads in order to minimize settling of spheroids and to enable even distribution in nanowells. Similar to the standard single-cell protocol, the iCELL8 chip was tightly sealed with a strongly adhesive imaging foil (TakaraBio). Instead of spinning cells to the bottom, spheroids were centrifuged upside-down to the foil (700 g, 5 min, 4 °C, decelerated break) in order to reduce the working distance and to avoid light reflections deep inside the well during imaging.

To further enhance imaging resolution, we used an inverted confocal laser-scanning microscope (Leica SP8) with a 10x objective (2 × 2 wells per field of view) instead of the standard and system-integrated fluorescence wide-field microscope.

Afterwards, spheroids were centrifuged to the bottom (700 g, 5 min, 4 °C) and chips were frozen at −80 °C. A 'filter file' was used to dispense reagents only in selected nanowells as described in the Rapid Development

Protocol (TakaraBio), with the exception that we adjusted the amount of Triton-X100 to a final well concentration of 1% for spheroids lysis. The timing of spheroid recovery and consequently the maximum spheroid size (that correlates with the number of cells per spheroid/well) should not exceed 100 µm as this might negatively influence RT efficiency. In addition, lysis reagents, concentration and duration might have to be adjusted for different culture models.

After in-chip reverse transcription and cDNA amplification (18 cycles), barcoded cDNA was pooled and processed to 3′-end sequencing libraries by the Nextera XT kit (Illumina) with specific adaptions described in the Rapid Development Protocol. Concentration and quality of cDNA and sequencing libraries was assessed by a fluorometer (Qubit) and by electrophoresis (Agilent Bioanalyzer high sensitivity DNA chips). Improved HT-pheno-seq paired-end iCELL8 libraries (21 + 70) were sequenced on an Illumina NextSeq 500 machine in high-output mode. The 'bottom control' chip without improved imaging was sequenced on a HiSeq 2000 machine with similar settings. However, this control was only used to assess library quality and not for further downstream analysis.

**Colon TICs spheroids.** *Cell culture.* Primary patient-derived colon tumor spheroid cultures were established as described previously[4]. Primary human colon cancer samples were obtained from Heidelberg University Hospital in accordance with the declaration of Helsinki. Informed consent on tissue collection was received from each patient, as approved by the Review Board of the Ethics Committee of the University Clinic Heidelberg. The culture used in this study was derived from a liver metastasis. Cells were cultured in 75 $cm^2$ ultra-low attachment flasks in advanced D-MEM/F-12 medium supplemented with Glucose (0.6%), 2 mM L-glutamine, 4 µg/ml heparin, 5 mM HEPES, 4 mg/ml BSA, 10 ng/ml FGF basic and 20 ng/ml EGF. Growth factors were added every 4 days and medium was exchanged every 4–8 days. For dissociation to single-cell suspensions, spheroid cultures were centrifuged for 5 min at 900 rpm and resuspended in 2–4 ml 0.25% Trypsin. To stimulate dissociation, shear forces were applied with a 1000 µl pipette every 5 min for 20 min in total. Subsequently, 4–8 ml stop solution (PBS with 20% heat inactivated and sterile filtered fetal bovine serum) was added and cells were centrifuged for 5 min at 900 rpm. For passaging, cells were then resuspended in medium, passed through a 40 µm strainer and counted.

*Reseeding assay.* To isolate, dissociate and reseed cells from big (70–100 µm) and small (20–40 µm) spheroids independently, we cultured colon spheroids for 10 days and performed a stepwise size exclusion by (reverse-) filtering with standard 100 µm, 70 µm, 40 µm and 20 µm cell strainers, respectively. Spheroids were dissociated to single-cell suspension as described above but passed through a 15 µm cell strainer and counted. Afterwards, 50,000 cells were seeded in 60 mm Ultra Low Attachment Culture Dishes (Corning). Growth factors were added every 4 days and cells cultured for 10 days. Culture dishes were shaken every day to avoid clustering of spheroids.

*Single-cell culture and pheno-seq of colon tumor spheroids.* For single-cell cultures of colon tumor cells, spheroids were dissociated to single-cell suspensions, passed through a 15 µm cell strainer and counted. Cells were cultured in Aggrewell 400 6-Well plates (StemCell Technologies) in which each well contains a standardized array of around 7000 inverse pyramidal shaped microwells with a size of 400 µm. For seeding, wells were pre-treated according to the manufacturer's instructions, washed once with PBS and once with medium. Subsequently, 3500 cells in 3 ml medium were added in a 45° angle to the wall of the well, which resulted in uniform distribution of single-cells in microwells after settling. Growth factors were added every 4 days and cells were cultured for 10 days, resulting in 300–400 spheroids (>20 µm) per 6-well. Spheroids from 4–6 plates (24–36 wells, 168,000–252,000 microwells) were harvested, pooled and washed once with FluoroBrite DMEM (Life Technologies, 900 rpm for 5 min).

HT-pheno-seq was performed as described for MCF10CA spheroids above, but with following modifications: In contrast to MCF10CA spheroids, colon spheroids did not require DSP fixation because spheroid recovery does not involve contact loss from reconstituted basement membrane (Matrigel). To minimize disassembly of spheroids during processing, cells were resuspended and dispensed in FluoroBrite DMEM instead of PBS.

**Microscopy and image analysis.** *Image processing and analysis.* Generally, acquired microscopy images were processed and analyzed using KNIME Image Processing (https://www.knime.com/community/image-processing, Version 3.2.1), ImageJ (https://imagej.nih.gov/ij/), R (Version 3.3.1)/R studio (https://www.rstudio.com/) and/or Graph Pad Prism 7 (https://www.graphpad.com /scientific-software/prism/). Generally, the ggplot2 package implemented in R and Graph Pad Prism 7 were used for data visualization and the PhenoSelect webtool design is based on the shiny package (https://shiny.rstudio.com). More detailed information on microscopy and image analysis can be found in the supplementary information file and in associated KNIME workflows deposited in the pheno-seq github repository (https://github.com/eilslabs/pheno-seq).

*HT-pheno-seq microscopy and image processing/analysis.* The following section describes the basic microscopy setup and imaging parameters for HT-pheno-seq as well as major steps for image processing and analysis. For further details, see supplementary methods.

For inverted imaging, 5184-nanowell iCELL8 chips were fixed on a metallic Chip Spinner (TakaraBio) with adhesive tape and placed into a standard plate holder. All wells were imaged upside-down automatically using an inverted Leica SP8 confocal microscope system. We used a 10×/0.30 air objective (Leica HC PL FLUOTAR) but images were acquired with 0.9x digital zoom to span 4 wells per field of view. Excitation was set to 405 and 552 nm and emission filter were set to receive signals between 415–485 nm (Hoechst) and 555–625 nm (CellTracker Red), respectively. A pre-defined HCS A template of the LAS X microscope software (Leica) was used for the grid design matching the chip dimensions. One image contained 512 × 512 pixels, with 2.53 µm pixel size. Scanning of one chip with these settings took approximately 30 minutes, resulting in 2 × 1296 images.

Images were automatically processed using KNIME/ImageJ for assigning images to their correct well positions, image cropping, spheroid detection and segmentation as well as feature extraction and quantification. The web-based shiny app 'PhenoSelect' was used for final selection of wells and for interactive analysis (see supplement for further details).

*Immunofluorescence.* MCF10CA cells cultured in 3D were prepared for immunofluorescence staining as described previously[28]. Briefly, cells were fixed in 24-wells with 2% Formaldehyde solution (Methanol-free, ThermoFisher) for 20 min at RT and washed twice with PBS. Cells were permeabilized with PBS + 0.5% TritonX-100 (Sigma) for 10 min and washed three times with PBS + 75 mg/ml Glycine (pH = 7.4, Sigma). Unspecific binding sites were blocked for 1 hour at RT with 10% goat serum in IF-wash solution (PBS + 5 mg/ml $NaN_3$, 10 mg/ml bovine serum albumin, 2% TritonX-100 and 0.4% Tween20, pH = 7.4, Sigma). Afterwards, primary antibodies in blocking solution were added and incubated at 4 °C overnight. The next day, cells were washed 3x with IF-wash and then incubated with fluorescently labeled secondary antibodies in blocking solution for 1 hour at RT if primary antibodies were unlabeled. Subsequently, cells were washed 3x with IF-wash and 2x with PBS and then incubated in PBS + 1 µg/ml Hoechst for 20 min at RT. Cells were again washed with PBS, removed from the surface and transferred into 8-well Nunc™ Lab-Tek™ Chamber Slides (ThermoFisher) for improved fluorescence detection. The following antibodies were used in this study: Rabbit anti-Vimentin antibody Alexa Fluor® 594 (1:100, EPR3776, abcam), mouse anti-β-Actin antibody (1:200, 8H10D10, Cell Signaling), Mouse anti-Cytokeratin 15 antibody (1:50, LHK15, ThermoFisher), Goat anti-mouse Alexa Fluor® 594 (1:200, Cell Signaling). 3 × 3 images per well (20 Z-stacks per position) were acquired automatically on a Zeiss LSM780 Axio Observer confocal microscope equipped with a 10x/0.3 air objective (Zeiss EC PLAN-NEOFLUAR) using a custom Zeiss VBA macro. Beside brightfield images, lasers and filters were set to measure fluorescence emitted from Hoechst (DNA) and from Alexa Fluor® 594-labeled antibodies. Images were analyzed using a custom KNIME workflow in which protein abundances per classified spheroid were defined as mean pixel intensity of the fluorescence signal emitted from labeled antibodies.

Z-stacks of whole mount stained MCF10CA spheroids were first merged by average intensity projection and a mask for single spheroids was created based on the Hoechst signal. Therefore, images were smoothed by Gaussian convolution (sigma = 2) and thresholded by Otsu's method. Labels were assigned to objects (spheroids) by connected component analysis and objects smaller than 300 and bigger than 800,000 pixels were filtered out to remove noise as well as segmentation artifacts. To compare expression of antibody targets between round and aberrant 3D phenotypes, single objects (spheroids) were manually classified as 'round' or 'aberrant' based on brightfield images. Protein abundances per spheroid were defined as mean pixel intensity of the fluorescence signal emitted from labeled antibodies.

*RNA FISH.* For histological preparation, 'big' (70–100 µm) and 'small' (70–100 µm) colon tumor spheroids derived from single-cells were isolated with (reverse-) filtering as described above. This step was added for histological preparation in order to distinguish between small spheroids and big spheroids that were sliced in peripheral regions. Spheroids were then fixed with 4% Formaldehyde solution for 20 min at 4 °C, washed twice with PBS and incubated in 30% sucrose at 4 °C overnight. The next day, spheroids were embedded in Neg-50™ and frozen in the gaseous phase of liquid nitrogen.

For both cultures, sectioning was performed at −20 °C on a cryostat (Leica) and 10 µm slices were mounted on Superfrost Plus slides (ThermoFisher). Embedded specimens and cryosections were stored at −80 °C until further use.

For highly sensitive RNA fluorescence *in-situ* hybridization (RNA-FISH), we employed the RNAscope® Fluorescent Multiplex Assay 2.0 (ACDbio). Cryosections were processed as described in the 'Sample Preparation Technical Note for Fixed Frozen Tissue' and the 'Fluorescent Multiplex Kit User Manual PART 2′. Briefly, cryosections were pretreated with Protease IV (ACDbio) for 15 min at RT. Afterwards, transcript-specific probes were hybridized at 40 °C for 90 min followed by stepwise hybridization of probes for signal amplification and fluorescent detection (Amp-1-FL – Amp-4-FL). Up to three transcripts were labeled by Alexa488, Atto550 and Atto647 fluorescent dyes. Following mRNA targeting probes were used: MYC (Atto550, #311761-C2), CD44 (Atto647, #311271-C3), TFF3 (Alexa488, #403101), PROX1 (Atto550, #530241-C2). Finally, cryosections were counterstained with DAPI, mounted in SlowFade™ Gold Antifade solution (ThermoFisher) and stored at 4 °C until further use.

RNA-FISH images were acquired on a Leica SP8 confocal laser-scanning microscope equipped with a 40x/1.30 oil objective (Leica HC APO CS2). Images of individual spheroids at 1024 × 1024 pixel resolution were generated semi-automatically using the 'Mark and Find' option in the Leica SP8 acquisition software. To cover the whole 10 µm cryosection height, a Z-range of 20 µm was acquired by 15 stacks (1.43 µm distance between frames). Lasers and filters were set to match fluorescent properties of DAPI and abovementioned dyes. For analysis of RNA-FISH imaging data we used a custom KNIME workflow in which we defined the relative transcript expression per spheroid as quantified pixel percentage that exceeds a calculated background threshold per spheroid.

Z-stacks acquired from histology slides were merged using maximum intensity projection and a mask for single spheroids was created using the DAPI signal. Briefly, acquired DAPI signals were smoothed by applying Gaussian convolution (sigma = 5) and a maximum filter with a radius of 12 pixels, resulting in individual masks for all spheroids within an image. Only the biggest object/spheroid was used for analysis if two or more objects were present in one image. To quantify transcript abundances (measured as fluorescence intensities derived from specifically labeled probes) we first accounted for background noise by fitting two local maxima, j and k, to the pixel intensity histogram of each spheroid using the 'intermodes' method in KNIME. Based on the determined probe-specific pixel intensity threshold between two maxima calculated as (j + k)/2, we defined the relative transcript expression per spheroid as quantified pixel percentage that exceeds this threshold per object.

**Sequencing data analysis.** *Pre-processing of RNA-seq data and library quality control.* An automated in-house workflow was established for pheno-seq and Fluidigm C1 scRNA-seq data pre-processing. Briefly, short read quality was evaluated using FastQC. For iCELL8 libraries, barcodes from the first 21 bp read were assigned to the well of origin with the Je demultiplexing suite[56]. Cutadapt was used to trim remaining primer sequences, Poly-A/T tails and low-quality ends (<25). In addition, since NextSeq (Illumina) encodes undetected base as incorrect 'G' with high quality, Cutadapt's '—nextseq-trim' option was used for correct quality trimming. Trimmed reads were mapped to the reference genome hs37d5 (1000 genomes project) using STAR aligner. Mapped BAM files were quantified using featureCounts with gencode v19 as reference annotation.

RNA-seq libraries that did not match the following criteria were filtered out: MCF10CA scRNA-seq: (i) > 300,000 reads, (ii) > 3000 detected genes (i.e. > 0 read count), (iii) < 10% mitochondrial reads; MCF10CA pheno-seq: (i) > 100,000 reads, (ii) > 2000 detected genes, (iii) < 15% mitochondrial reads; Colon spheroid pheno-seq: (i) > 200,000 reads, (ii) > 3000 detected genes, (iii) < 15% mitochondrial reads.

In order to compare the performance of scRNA-seq and pheno-seq methods in detecting genes, MCF10CA sequencing libraries were downsampled to 100,000 reads by a custom R script.

Wells/Spheroids with imaging artifacts (e.g. segmentation errors) were removed if detected during combined downstream analysis.

*PAGODA/SCDE subpopulation and differential expression analysis.* To identify expression signatures that separate distinct cellular subpopulations, we analyzed transcriptional heterogeneity by pathway and gene set overdispersion analysis (PAGODA/SCDE-package[33]). First, genes with less than 10 mapped reads in the whole dataset were not considered for further analysis. Next, PAGODA constructs error models for individual cells using a binominal/Poisson mixture model, thereby controlling for technical aspects of variability, like effective sequencing depth, drop-out rate and amplification noise. For K-nearest neighbor error modelling, k was set to 30 (except for the full-length pheno-Seq dataset: k = 3), and the minimum number of reads required to be considered non-failed was set to 2. Afterwards, PAGODA performs weighted principal component analysis (wPCA) on annotated and *de-novo* identified gene sets in order to identify those that exhibit statistically significant variability. Generally, the scores for the first principal component are presented if not stated otherwise. Annotated hallmark (H) and gene ontology (GO_C5) gene sets were derived from the Molecular Signature Database (MSigDB). *De-novo* gene sets were identified by hierarchical clustering (Ward method; dendrogram was cut into 150 clusters). Pathway overdispersion was calculated as Z-score relative to the genome-wide model and corrected Z-scores (cZ) were computed using multiple hypothesis testing using the Holm procedure. Hierarchical clustering is then performed on the top significant aspects of heterogeneity and redundant aspects of heterogeneity were grouped with a similarity threshold of 0.7. Up to 10 top significant aspects were used for visualization. In addition, 2D t-SNE maps[57] were generated based on PAGODA's weighted Pearson correlation distances. Finally, the following confounding expression signatures (e.g. technical aspect or cell cycle influence) were removed using the 'pagoda.substract.aspect' function:

(1) For all datasets we corrected for the influence of gene coverage (estimated as a number of genes with non-zero magnitude per cell)
(2) MCF10CA scRNA-seq: GO_REGULATION_OF_CELL_CYCLE and HALLMARK _G2M_CHECKPOINT;
(3) MCF10CA HT-pheno-seq: GO_ NUCLEOSIDE_MONOPHOSPHATE_ METABOLIC _PROCESS, GO_MITOCHONDRIAL_ENVELOPE, GO_STRUCTURAL _MOLECULE _ACTIVITY, GO_ HOMEOSTATIC_PROCESS and associated *de-novo* identified gene sets.

Differentially expressed genes (MCF10CA: fold change >1.3; adjusted p-value < 0.1; CRC spheroids: fold change >1.5; adjusted p-value < 0.05) between detected subpopulations that refer to observed visual phenotypes (k-means clustering, k = 2) were identified by the SCDE-package[37].

*In-silico reconstruction of synthetic pheno-seq expression profiles from single-cell data.* Synthetic spheroid expression profiles were reconstructed from scRNA-seq data by randomly dividing cells either derived from round and aberrant phenotypes in four groups each in four independent randomizations. Read counts for each gene were then averaged over each group, resulting in eight synthetic spheroid profiles (4 round and 4 aberrant) that were then analyzed by PAGODA similar to the full-length pheno-seq dataset.

*Deconvolution of the CRC spheroid dataset by maximum likelihood inference.* In order to infer heterogeneous regulatory states informative for single cell expression by deconvolution, we adapted a maximum likelihood inference approach initially developed to identify cell-to-cell heterogeneities from random 10-cell samples[45] (Stochastic Profiling, Fig. 3a). The adapted algorithm uses the estimated cell numbers per spheroid to fit two log-normal distributions (LN-LN model) to given 'mixed-n' datasets in order to identify genes with bimodal expression pattern at the single-cell level (Stochastic Profiling). Here, we allowed each sample to consist of different numbers of cells (implemented in the R package stochprofML version 2.0: https://github.com/fuchslab/stochprofML).

The algorithm assumes that the expression of a spheroid linearly scales with its cell number. We approximated absolute counts per spheroid by using estimated cell numbers derived from light sheet microscopy and image analysis and normalized pheno-seq data as follows: First, counts per spheroid were divided by the respective estimated cell number, and the minimal average mRNA count per cell was determined (2374.644). Afterwards we downsampled the whole dataset to 2300 counts per cell resulting in a perfect correlation of mRNA counts and cell

numbers. (Supplementary Fig. 9b). The downsampled dataset was filtered by removing genes with less than one count per well on average over the original CRC spheroid dataset and genes with less than 5 counts in at least two wells, leaving 13,868 genes that are taken into account during the profiling procedure. To avoid problems with zeros and log-normal distributions, all zeros were transformed to 0.1.

*Scoring of pheno-seq data for subtype-specific gene expression signatures.* First, meta-signatures for predicted single cell subtypes (stem, transit amplifying and terminally differentiated) were defined as the averaged expression of the top 20 genes most highly correlated with PROX1 (stem) or TFF3 (Tdiff). The TA signature was defined as average expression of ribosomal genes identified by pheno-seq deconvolution (n = 24 genes). We used control random gene sets as a background model in order to control for technical confounders[20]. To link subtype-specific expression to pheno-seq clusters, downsampled spheroid expression profiles (see Stochastic Profiling normalization) were scored for defined signatures. Finally, signature scores for the two identified pheno-seq clusters ('big' and 'small'-phenotype) were compared using unpaired two-tailed Students t-test.

*Statistical analysis and visualization.* Statistical analysis and visualization of sequencing data was done in R (Version 3.3.1) or R studio (https://www.rstudio.com/) using PAGODA/SCDE[33], (Version 2.3), ggplot2, ComplexHeatmaps[58], the stats package (R version 3.3.1), stochprofML (R version 3.4.1) and in Graph Pad Prism 7 (https://www.graphpad.com/scientific-software/prism/). Gene set enrichment analysis was done by computing overlaps between identified class-specific signatures and gene sets derived from the Molecular Signature Database[38] (MSigDB, https://software.broadinstitute.org/gsea/msigdb).

## Data and Code Availability

Raw sequencing data for MCF10CA are accessible at the European Nucleotide Archive (https://www.ebi.ac.uk/ena) under Accession Number PRJEB26737.

Colon tumor spheroid raw sequencing data have been deposited at the European Genome-Phenome Archive (http://www.ebi.ac.uk/ega/) under Accession Number EGAS00001002999.

All KNIME image analysis workflows, R code for PhenoSelect and PAGODA/SCDE RNA-seq analysis as well as a download link for MCF10CA HT-pheno-seq image data with all necessary components to run the pre-processing workflow and/or the PhenoSelect web app can be found in the pheno-seq github repository (https://github.com/eilslabs/pheno-seq). Information on the automated in-house RNA-seq workflow is available upon request. The newest version of stochProfML 3.4.1 can be found under: https://github.com/fuchslab/stochprofML.

## References


1. Weiswald, L. B., Bellet, D. & Dangles-Marie, V. Spherical Cancer Models in Tumor Biology. *Neoplasia (United States)* **17**, 1–15 (2015).
2. Fatehullah, A., Tan, S. H. & Barker, N. Organoids as an *in vitro* model of human development and disease. *Nat. Cell Biol.* **18**, 246–254 (2016).
3. Pampaloni, F., Reynaud, E. G. & Stelzer, E. H. K. The third dimension bridges the gap between cell culture and live tissue. *Nat. Rev. Mol. Cell Biol.* **8**, 839–845 (2007).
4. Dieter, S. M. *et al.* Distinct types of tumor-initiating cells form human colon cancer tumors and metastases. *Cell Stem Cell* **9**, 357–365 (2011).
5. Borten, M. A., Bajikar, S. S., Sasaki, N., Clevers, H. & Janes, K. A. Automated brightfield morphometry of 3D organoid populations by OrganoSeg. *Sci. Rep.* **8**, 5319 (2018).
6. Serra, D. *et al.* Self-organization and symmetry breaking in intestinal organoid development. *Nature*, https://doi.org/10.1038/s41586-019-1146-y (2019).
7. Sachs, N. *et al.* A Living Biobank of Breast Cancer Organoids Captures Disease Heterogeneity. *Cell* **172**, 373–386.e10 (2018).
8. Seino, T. *et al.* Human Pancreatic Tumor Organoids Reveal Loss of Stem Cell Niche Factor Dependence during Disease. *Cell Stem Cell* **22**, 454–467.e6 (2018).
9. Tsai, J. H. & Yang, J. Epithelial – mesenchymal plasticity in carcinoma metastasis. *Genes Dev.* **27**, 2192–2206 (2013).
10. Bhang, H. E. C. *et al.* Studying clonal dynamics in response to cancer therapy using high-complexity barcoding. *Nat. Med.* **21**, 440–448 (2015).
11. McGranahan, N. & Swanton, C. Clonal Heterogeneity and Tumor Evolution: Past, Present, and the Future. *Cell* **168**, 613–628 (2017).
12. Mazor, T., Pankov, A., Song, J. S. & Costello, J. F. Intratumoral Heterogeneity of the Epigenome. *Cancer Cell* **29**, 440–451 (2016).
13. Junttila, M. R. & De Sauvage, F. J. Influence of tumour micro-environment heterogeneity on therapeutic response. *Nature* **501**, 346–354 (2013).
14. Shaffer, S. M. *et al.* Rare cell variability and drug-induced reprogramming as a mode of cancer drug resistance. *Nature* **546**, 431–435 (2017).
15. Bedard, P. L., Hansen, A. R., Ratain, M. J. & Siu, L. L. Tumour heterogeneity in the clinic. *Nature* **501**, 355–364 (2013).
16. Kolodziejczyk, A. A., Kim, J. K., Svensson, V., Marioni, J. C. & Teichmann, S. A. The Technology and Biology of Single-Cell RNA Sequencing. *Mol. Cell* **58**, 610–620 (2015).
17. Haque, A., Engel, J., Teichmann, S. A. & Lönnberg, T. A practical guide to single-cell RNA-sequencing for biomedical research and clinical applications. *Genome Med.* **9**, 75 (2017).
18. Patel, A. P. *et al.* Single-cell RNA-seq highlights intratumoral heterogeneity in primary glioblastoma. *Science (80-.).* **344**, 1396–1401 (2014).
19. Tirosh, I. *et al.* Dissecting the multicellular ecosystem of metastatic melanoma by single-cell RNA-seq. *Science (80-.).* **352**, 189–196 (2016).
20. Puram, S. V. *et al.* Single-Cell Transcriptomic Analysis of Primary and Metastatic Tumor Ecosystems in Head and Neck Cancer. *Cell* **171**, 1611–1624.e24 (2017).
21. Nichterwitz, S. *et al.* Laser capture microscopy coupled with Smart-seq. 2 (LCM-seq) for robust and efficient transcriptomic profiling of mouse and human cells. *Nat. Commun.* **7**, 1–11 (2016).
22. Ståhl, P. L. *et al.* Visualization and analysis of gene expression in tissue sections by spatial transcriptomics. *Science (80-.).* **353**, 78–82 (2014).
23. Rodriques, S. G. *et al.* Slide-seq: A scalable technology for measuring genome-wide expression at high spatial resolution. *Science (80-.).* **363**, 1463–1467 (2019).

24. Eng, C.-H. L. *et al*. Transcriptome-scale super-resolved imaging in tissues by RNA seqFISH+. *Nat.* **2019**, 1, https://doi.org/10.1038/s41586-019-1049-y (2019).
25. Wang, X. *et al*. Three-dimensional intact-tissue sequencing of single-cell transcriptional states. **5691**, 1–18 (2018).
26. Marella, N., Malyavantham, K. & Wang, J. Cytogenetic and cdna microarray expression analysis of MCF10A human breast cancer progression cell lines. *Cancer Res.* **69**, 5946–5953 (2009).
27. Debnath, J. & Brugge, J. S. Modelling glandular epithelial cancers in three-dimensional cultures. *Nat. Rev. Cancer* **5**, 675–688 (2005).
28. Debnath, J., Muthuswamy, S. K. & Brugge, J. S. Morphogenesis and oncogenesis of MCF-10A mammary epithelial acini grown in three-dimensional basement membrane cultures. *Methods* **30**, 256–268 (2003).
29. Santner, S. J. *et al*. Malignant MCF10CA1 cell lines derived from premalignant human breast epithelial MCF10AT cells. *Breast Cancer Res. Treat.* **65**, 101–110 (2001).
30. Strickland, L. B., Dawson, P. J., Santner, S. J. & Miller, F. R. Progression of premalignant MCF10AT generates heterogeneous malignant variants with characteristic histologic types and immunohistochemical markers. *Breast Cancer Res. Treat.* **64**, 235–240 (2000).
31. Gao, R. *et al*. Nanogrid single-nucleus RNA sequencing reveals phenotypic diversity in breast cancer. *Nat. Commun.* **8**, 228 (2017).
32. Attar, M. *et al*. A practical solution for preserving single cells for RNA sequencing. *Sci. Rep.* **8**, 2151 (2018).
33. Fan, J. *et al*. Characterizing transcriptional heterogeneity through pathway and gene set overdispersion analysis. *Nat. Methods* **13**, 241–244 (2016).
34. Ye, X. & Weinberg, R. A. Epithelial-Mesenchymal Plasticity: A Central Regulator of Cancer Progression. *Trends Cell Biol.* **25**, 675–686 (2015).
35. Liberzon, A. *et al*. The Molecular Signatures Database Hallmark Gene Set Collection. *Cell Syst.* **1**, 417–425 (2015).
36. Bach, K. *et al*. Differentiation dynamics of mammary epithelial cells revealed by single-cell RNA sequencing. *Nat. Commun*. **8** (2017).
37. Kharchenko, P. V., Silberstein, L. & Scadden, D. T. Bayesian approach to single-cell differential expression analysis. *Nat. Methods* **11**, 740–742 (2014).
38. Subramanian, A. *et al*. Gene set enrichment analysis: A knowledge-based approach for interpreting genome-wide expression profiles. *Proc. Natl. Acad. Sci.* **102**, 15545–15550 (2005).
39. Van Den Brink, S. C. *et al*. Single-cell sequencing reveals dissociation-induced gene expression in tissue subpopulations. *Nat. Methods* **14**, 935–936 (2017).
40. Giessler, K. M. *et al*. Genetic subclone architecture of tumor clone-initiating cells in colorectal cancer. *J. Exp. Med.* **214**, 2073–2088 (2017).
41. Dieter, S. M., Glimm, H. & Ball, C. R. Colorectal cancer-initiating cells caught in the act. *EMBO Mol. Med.* **9**, 856–858 (2017).
42. Haber, A. L. *et al*. A single-cell survey of the small intestinal epithelium. *Nature* **551**, 333–339 (2017).
43. Dalerba, P. *et al*. Single-cell dissection of transcriptional heterogeneity in human colon tumors. *Nat. Biotechnol.* **29**, 1120–1127 (2011).
44. Takebe, N. *et al*. Targeting Notch, Hedgehog, and Wnt pathways in cancer stem cells: Clinical update. *Nat. Rev. Clin. Oncol.* **12**, 445–464 (2015).
45. Bajikar, S. S., Fuchs, C., Roller, A., Theis, F. J. & Janes, K. A. Parameterizing cell-to-cell regulatory heterogeneities via stochastic transcriptional profiles. *Proc. Natl. Acad. Sci.* **111**, E626–E635 (2014).
46. Smillie, C. S. *et al*. Rewiring of the cellular and inter-cellular landscape of the human colon during ulcerative colitis. *bioRxiv* 455451, https://doi.org/10.1101/455451 (2019).
47. Grün, D. *et al*. Single-cell messenger RNA sequencing reveals rare intestinal cell types. *Nature* **525**, 251–255 (2015).
48. TakaraBio, https://www.takarabio.com/learning-centers/automation-systems/smarter-icell8-introduction/technical-notes/full-length-transcriptome-analysis (2019).
49. Yan, K. S. *et al*. Intestinal Enteroendocrine Lineage Cells Possess Homeostatic and Injury-Inducible Stem Cell Activity. *Cell Stem Cell* **21**, 78–90.e6 (2017).
50. Wiener, Z. *et al*. Prox1 promotes expansion of the colorectal cancer stem cell population to fuel tumor growth and ischemia resistance. *Cell Rep.* **8**, 1943–1956 (2014).
51. Ragusa, S. *et al*. PROX1 promotes metabolic adaptation and fuels outgrowth of Wnthigh metastatic colon cancer cells. *Cell Rep.* **8**, 1957–1973 (2014).
52. Khoo, B. L. *et al*. Expansion of patient-derived circulating tumor cells from liquid biopsies using a CTC microfluidic culture device. *Nat. Protoc.* **13**, 34–58 (2018).
53. Buenrostro, J. D. *et al*. Single-cell chromatin accessibility reveals principles of regulatory variation. *Nature* **523**, 486–490 (2015).
54. Datlinger, P. *et al*. Pooled CRISPR screening with single-cell transcriptome readout. *Nat. Methods* **14**, 297–301 (2017).
55. Goldstein, L. D. *et al*. Massively parallel nanowell-based single-cell gene expression profiling. *BMC Genomics* **18**, 1–10 (2017).
56. Girardot, C., Scholtalbers, J., Sauer, S., Su, S. Y. & Furlong, E. E. M. Je, a versatile suite to handle multiplexed NGS libraries with unique molecular identifiers. *BMC Bioinformatics* **17**, 4–9 (2016).
57. van der Maaten, L. & Hinton, G. Visualizing Data using t-SNE. *J. Mach. Learn. Res.* **9**, 2579–2605 (2008).
58. Gu, Z., Eils, R. & Schlesner, M. Complex heatmaps reveal patterns and correlations in multidimensional genomic data. *Bioinformatics* **32**, 2847–2849 (2016).


## Acknowledgements

We thank David Ibberson (CellNetworks Deep Sequencing Core Facility, Heidelberg University) for NGS services, Daniel Liber and Marizela Kulisic (TakaraBio) for technical support for the iCELL8 system, Henrik Kaessmann and his group (ZMBH, Heidelberg University) for support and helpful discussions regarding the iCELL8 system and single cell analysis, Lorenz Maier (Theoretical Bioinformatics, DKFZ) for help with KNIME, Katharina Jechow (Theoretical Bioinformatics, DKFZ) for technical laboratory support, Claudia Ernst and Niels Grabe (Hamamatsu TIGA Center, Heidelberg University) for help with histological preparation, Naveed Ishaque (Theoretical Bioinformatics, DKFZ) for assistance in RNA-seq data analysis and Dominik Niopek, Luca Tosti, Julia Neugebauer, Teresa Krieger and Lorenz Chua (Theoretical Bioinformatics, DKFZ) for critically revising the manuscript. Primary human colon cancer samples were obtained from Heidelberg University Hospital in accordance with the declaration of Helsinki. Informed consent on tissue collection was received from each patient, as approved by the Review Board of the Ethics Committee of the University Clinic Heidelberg. ST is recipient of the stipend for the PhD program of the Helmholtz International Graduate School for Cancer Research (DKFZ, Heidelberg). This study was supported by the Helmholtz International Graduate School for Cancer Research, the iMed Program (Helmholtz Association), the BMBF-funded Heidelberg Center for Human Bioinformatics (HD-HuB) within the German Network for Bioinformatics Infrastructure (de.NBI) (#031A537A,

#031A537C), the DFG (SFB873), the EU framework programme Horizon2020 (TRANSCAN-2 ERA-NET), the German Cancer Aid (Colon-Resist-Net), NCT3.0_2015.4 TransOnco. and NCT3.0_2015.54 DysregPT, the German Research Foundation (DFG) within the Collaborative Research Centre 1243, Subproject A17, the BMBF (grant # 01ZX1711A) and the Helmholtz Association (Incubator grant sparse2big, grant # ZT-I-0007). DKFZ-HIPO provided technical support and funding through Grant No. HIPO-H012.

## Author Contributions

S.M.T. and C.C. conceived the study, S.M.T., C.C., H.G. and R.E. designed experiments; S.M.T. performed 3D cell culture experiments, IF/RNA-FISH stainings and iCELL8 sample and library preparation; S.M.T. and F.P. performed confocal microscopy; B.E. performed light-sheet microscopy; S.M.T. and F.P. developed the HT-pheno-seq imaging protocol; F.P. developed the image processing pipeline and PhenoSelect; FP and MW performed image analysis; J.P.M. and S.M.T. performed Fluidigm C1 scRNA-seq experiments and J.P.M. generated C1 sequencing libraries; J.P., L.A., S.M.T., Z.G., T.K. and S.S. analyzed RNA-seq data; L.A., C.F. and F.J.T. developed and applied the adapted maximum likelihood inference deconvolution approach; C.B. and H.G. generated and characterized the colon spheroid cultures and contributed experimental and clinical expertise; K.R., M.S., M.G. and I.G. provided advice on sequencing experiments and analysis. M.G. and I.G. contributed expertise on NGS and sample processing. S.M.T. and C.C. wrote the manuscript. All authors revised and approved the manuscript.

## Additional Information

**Supplementary information** accompanies this paper at https://doi.org/10.1038/s41598-019-48771-4.

**Competing Interests:** The authors declare no competing interests.

**Publisher's note:** Springer Nature remains neutral with regard to jurisdictional claims in published maps and institutional affiliations.

# Supplementary information

## Pheno-seq – linking visual features to gene expression in 3D cell culture systems

*Stephan M. Tirier[2,3,7*], Jeongbin Park[1,3], Friedrich Preußer[2,3,4*], Lisa Amrhein[5,6], Zuguang Gu[3,8], Simon Steiger[2,3], Jan-Philipp Mallm[2,7,8], Teresa Krieger[1,2,3], Marcel Waschow[2,3], Björn Eismann[2,3], Marta Gut[9,10], Ivo G. Gut[9,10], Karsten Rippe[2,7], Matthias Schlesner[3,11], Fabian Theis[5,6], Christiane Fuchs[5,6,12], Claudia R. Ball[13], Hanno Glimm[13,14], Roland Eils[1,2,3,8,15], Christian Conrad[1,2,3,8,†]*

## Affiliations

[1]Digital Health Center, Berlin Institute of Health (BIH)/Charité-Universitätsmedizin Berlin, Berlin, Germany

[2]Center for Quantitative Analysis of Molecular and Cellular Biosystems (BioQuant), University of Heidelberg, Heidelberg, Germany.

[3]Division of Theoretical Bioinformatics, German Cancer Research Center (DKFZ), Heidelberg, Germany.

[4]Max Delbrück Center for Molecular Medicine, Berlin Institute for Medical Systems Biology, Berlin, Germany

[5]Helmholtz Zentrum München - German Research Center for Environmental Health, Institute of Computational Biology, Munich, Neuherberg, Germany

[6]Department of Mathematics, Technische Universität München, Munich, Germany

[7]Division of Chromatin Networks, German Cancer Research Center (DKFZ), Heidelberg, Germany.

[8]Heidelberg Center for Personalized Oncology, DKFZ-HIPO, DKFZ, Heidelberg, Germany.

[9]CNAG-CRG, Centre for Genomic Regulation, Barcelona Institute of Science and Technology, Barcelona, Spain.

[10]Universitat Pompeu Fabra, Barcelona, Spain.

[11]Bioinformatics and Omics Data Analytics, German Cancer Research Center (DKFZ), Heidelberg, Germany.

[12]Faculty of Business Administration and Economics, Bielefeld University, Bielefeld, Germany.

[13]Department of Translational Oncology, NCT Dresden, University Hospital, Carl Gustav Carus, Technische Universität Dresden, Dresden and DKFZ, Heidelberg, Germany

[14]German Cancer Consortium, Heidelberg, Germany.

[15]Health Data Science Unit, University Hospital Heidelberg, Heidelberg, Germany.

[†]Corresponding author: christian.conrad@bihealth.de

*Current address

Keywords: 3D cell culture, tumor cell heterogeneity, single cell analysis, gene expression deconvolution, spheroid image analysis

## Supplementary figures and tables

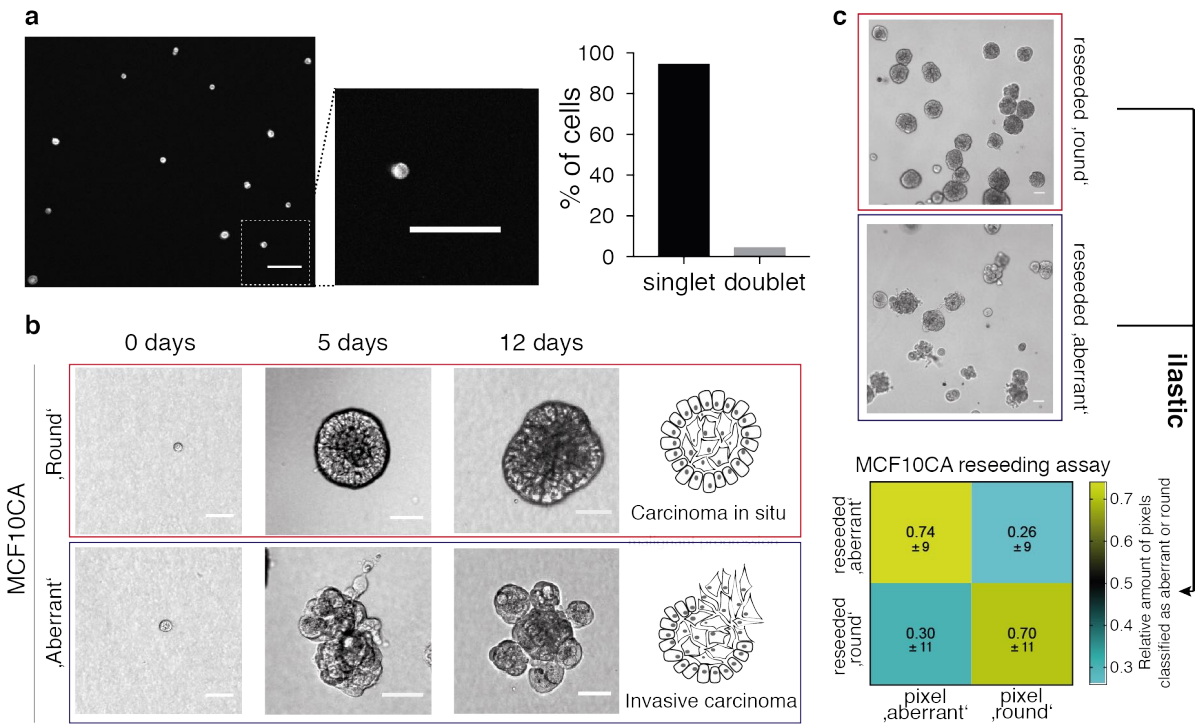


**Supplementary Figure 1 | Heterogeneous 3D breast cancer model MCF10CA** **(a)** Single-cell seeding efficiency assessed by image analysis. Left: Example image of CellTacker Red stained and seeded cells (scale bar: 100 µm). Middle: Magnified image that corresponds to dashed box in left image. Right: Quantified cell singlets and doublets after seeding (289 objects in total). **(b)** Brightfield microscopy images of heterogeneous MCF10CA spheroids after 0, 5 and 12 days of culture in Matrigel, thereby reflecting histological characteristics of key steps during malignant progression of breast cancer (Brightfield, scale bar 50 µm). Red box: 'round' phenotype; Blue box: 'aberrant' phenotype. **(c)** Independent reseeding of isolated 'round' and 'aberrant' spheroid phenotypes and quantification after regrowth by 'ilastic' machine learning based on pixel classification. Lower: Spheroid classification confusion matrix. Heatmap reflecting classified pixels as aberrant or round after reseeding (four replicates, indicated are relative pixel numbers and standard error of the mean below). Upper: Example images of reseeded MCF10CA 'round' and 'aberrant' spheroids 5 days after reseeding (scale bar: 50 µm)

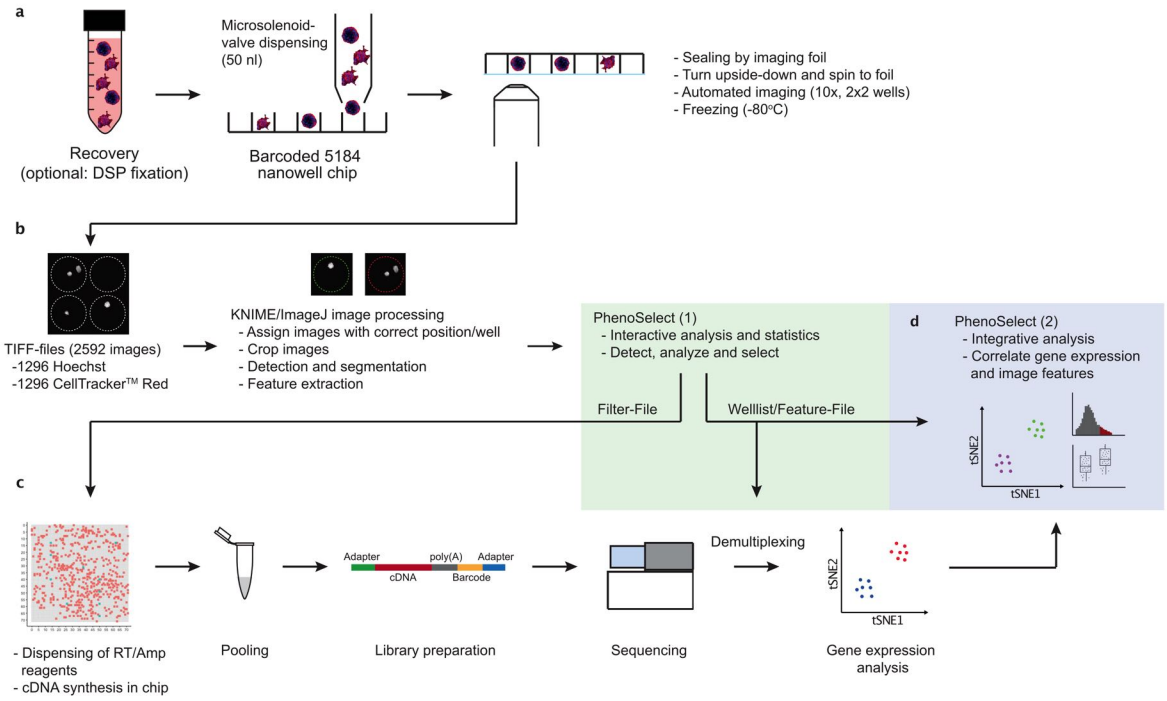


**Supplementary Figure 2 | Detailed pheno-seq workflow. (a)** After staining and recovery (optional: DSP fixation), spheroids are distributed into a nanowell chip by a Microsolenoid-valve dispenser (50 nl per well). To improve imaging quality, spheroids are centrifuged upside-down to the foil and automatically imaged by an inverted confocal microscope. The chip is then frozen at -80°C. **(b)** Images are processed using a custom-made image processing pipeline in KNIME/ImageJ. A Shiny-based web-app (PhenoSelect) enables interactive analysis and selection based on quantified image features. **(c)** A filter-file generated by PhenoSelect is used to dispense RT/Amp reagents only in selected wells. cDNA generation and amplification are performed in the chip. After pooling of barcoded cDNA, 3´-library generation and next generation sequencing, resulting raw data can be de-multiplexed using internal barcodes listed in the welllist/feature-file generated with PhenoSelect. **(d)** Combined image analysis enables combined analysis of gene expression and image features.

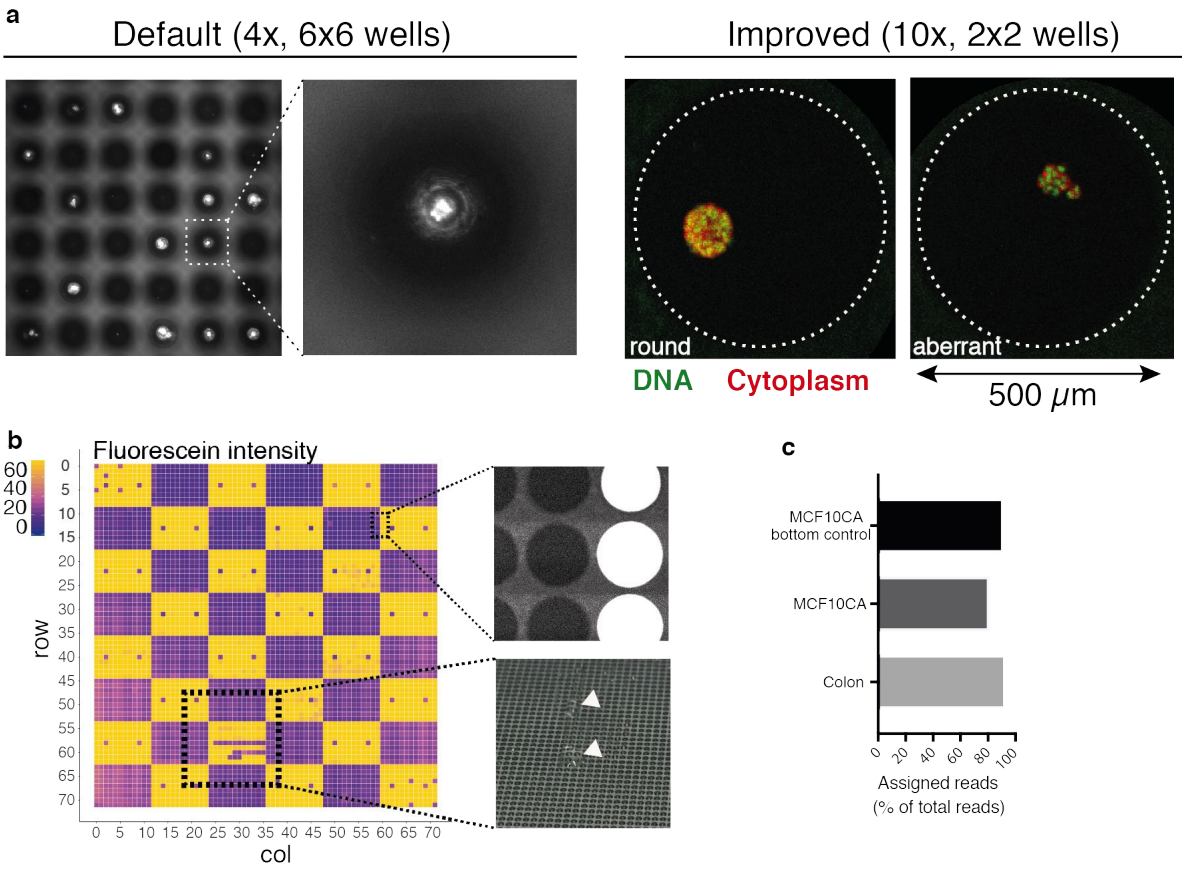


**Supplementary Figure 3 | Technical adaptions and controls for pheno-seq and PhenoSelect webtool. (a)** Comparison of images acquired by the default microscope with 4x objective, capturing 6x6 wells per image (spheroid nuclei are stained with Hoechst dye), and higher resolution microscopy (Confocal Leica SP8) with 10x objective, capturing 2x2 wells per image (spheroids are stained with Hoechst dye and CellTracker Red CMTPX). **(b)** Leakage analysis by patterned Fluorescein dispensing. Average fluorescence intensity is plotted onto 72x72 well grid that corresponds to nanowell chip architecture (left). For better visualization, all average intensity values exceeding 77 were set to maximum in the color code scheme. Top right: Example image showing the border between wells that have been filled with PBS or PBS with Fluorescein. Lower right: Macroscopic image of nanowell surface with droplets, showing rare dispensing errors that are also reflected by absence of Fluorescein signal at the respective position. **(c)** High percentage of reads that only map to selected well barcodes excludes severe leakage of barcoded Poly-T primers upon centrifugation of spheroids to the foil.

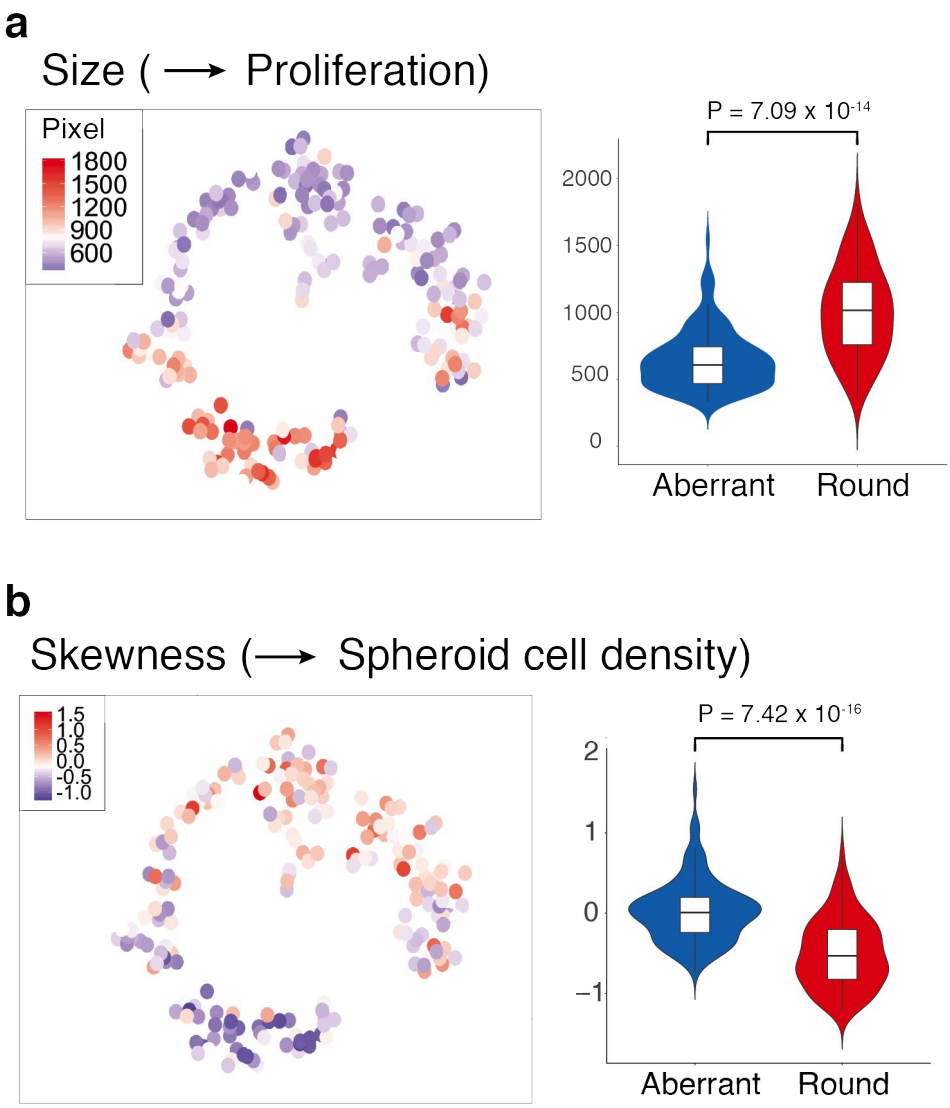


**Supplementary Figure 4 | Additional image features that are linked to gene expression clusters in MCF10CA pheno-seq data (a and b)** PAGODA 2D tSNE embedding of MCF10CA pheno-seq dataset colored for image features 'size' (a) and 'skewness' (b) and associated Violin plots for image feature quantification per cluster (k-means clustering: k=2; violin center-line: median; box limits: first and third quartile; whiskers: ±1.5 IQR; Indicated *P*-values from unpaired two-tailed Students t-test). Image feature associations can be interpreted according to the biological background (proliferation and cell density)

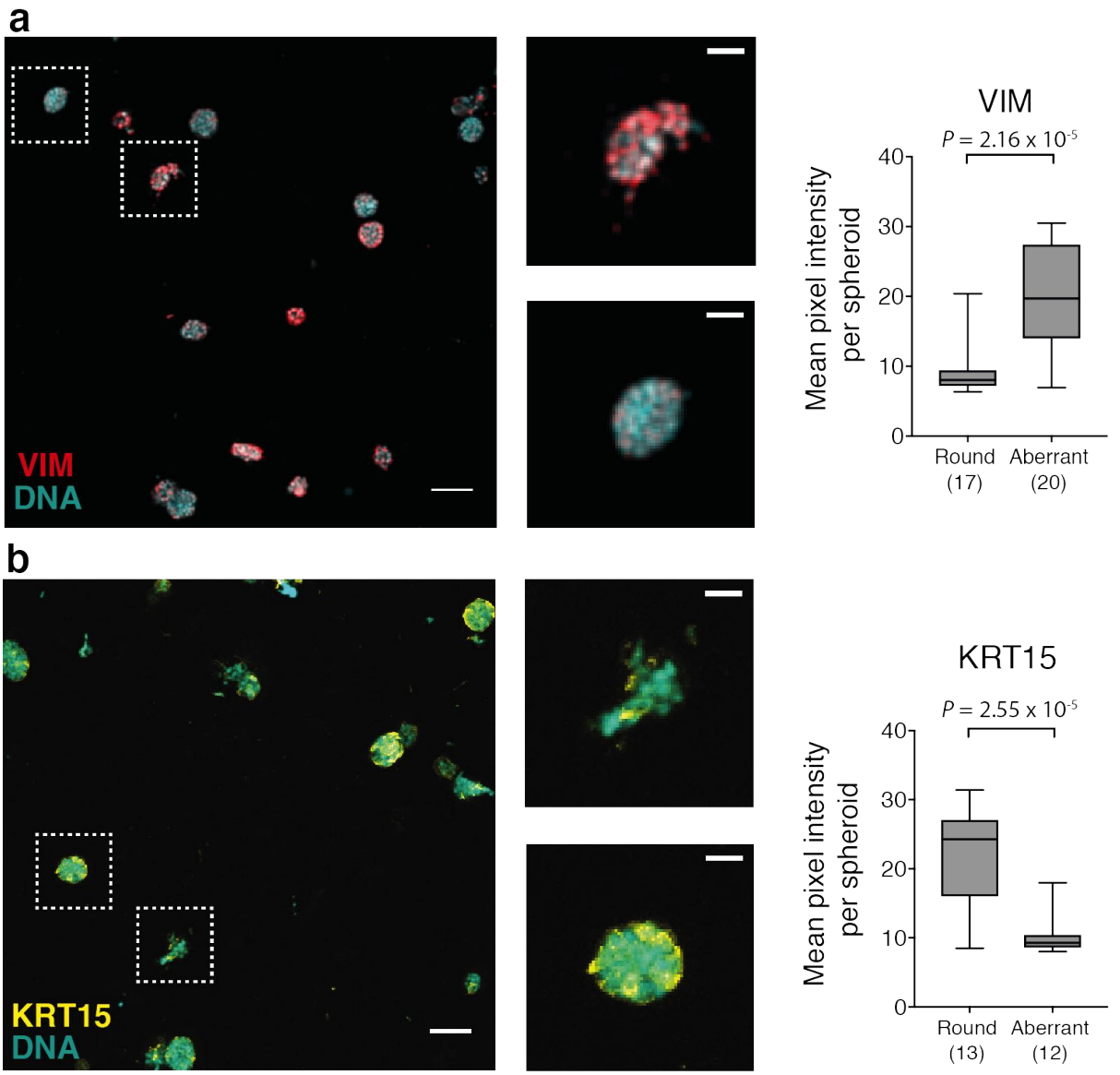


**Supplementary Figure 5 | Validation of RNA-seq data by quantitative fluorescence microscopy. (a and b)** Immunofluorescence staining with primary antibodies targeting VIM and KRT15 (b). Images represent Z-projections of whole mount spheroid immunofluorescence. Plotted values reflect the mean pixel intensity per classified spheroid of the respective class. Dashed boxes in overview images (scale bar 100 µm) correspond to magnified images beside (scale bar 30 µm). Samples are counterstained with Hoechst dye to visualize nuclei (Hoechst: cyan; KRT15: yellow; VIM: red). (Box plot center-line: median; box limits: first and third quartile; whiskers: min/max values; Indicated *P*-values from unpaired two-tailed Students t-test; Numbers of samples indicated on x-axis under respective class).

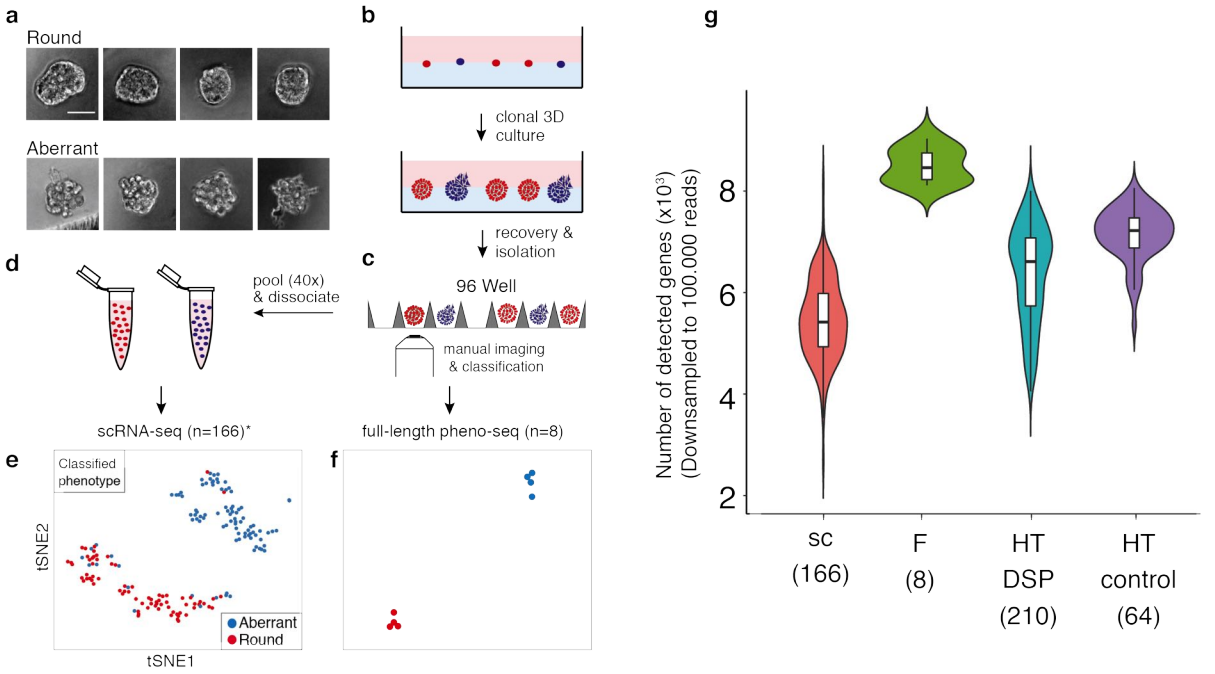


**Supplementary Figure 6 | Full-length scRNA-seq and full-length pheno-seq based on manually isolated spheroids.** **(a)** Brightfield images of clonal MCF10CA spheroids (phenotype classes 'round' and 'aberrant') after isolation from Matrigel (scale bar 50 µm). **(b and c)** Workflow overview for the culture, recovery (b) and isolation (c) of clonal spheroids for the identification of morphology-specific gene expression for full length pheno-seq/scRNA-seq. **(d)** Indirect phenotype – transcriptome correlation by scRNA-seq using cells isolated from multiple (40) spheroids of one annotated morphology phenotype. **(e)** tSNE visualization of 166 scRNA-seq (*cell-cycle corrected) full-length expression profiles of cells derived from manually isolated round and aberrant spheroids. Coloring based on phenotype classification. **(f)** tSNE visualization of 8 full-length pheno-seq expression profiles based on isolated and processed single spheroids. Same coloring as presented in (e). **(g)** Number of detected genes in downsampled scRNA-seq and pheno-seq libraries (sc: scRNA-seq; F: full-length pheno-seq; HT-DSP: high-throughput pheno-seq combined with dithio-bis(succinimidyl) propionate fixation; HT-control: HT-pheno-seq bottom control). Numbers of samples indicated on x-axis under respective strategy.

ô

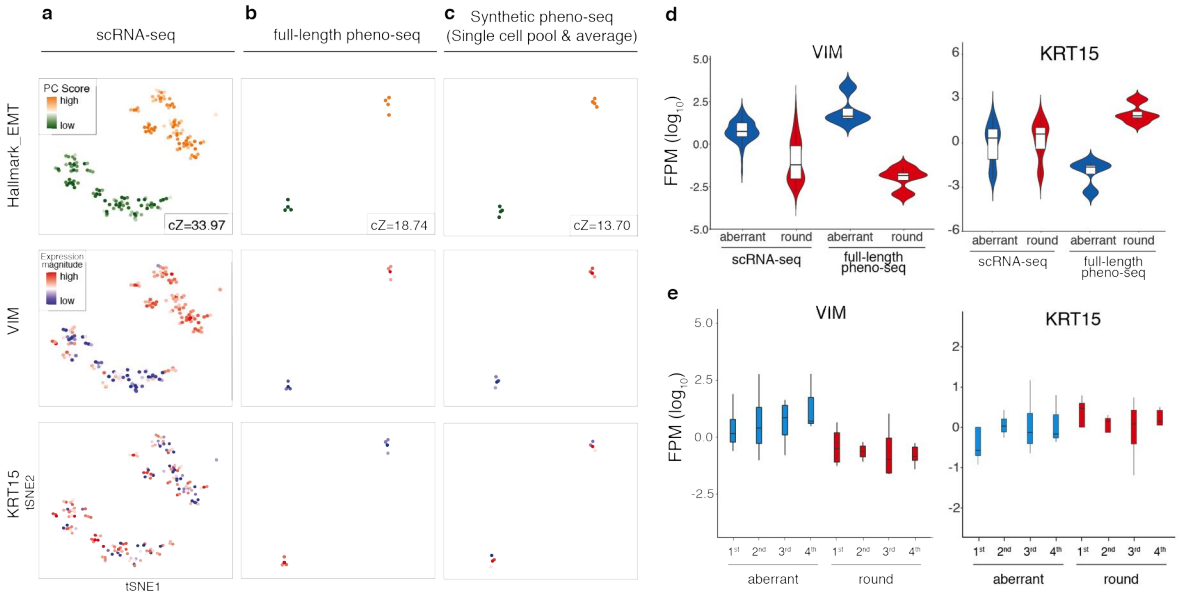


**Supplementary Figure 7 | 'Round' spheroid marker KRT15 is missed by scRNA-seq (a,b,c)** PAGODA tSNE visualizations of MCF10CA scRNA-seq (a), full-length pheno-seq (b) and synthetic pheno-seq (c, based on averaged single cell data). Datasets are colored by PC scores for HALLMARK_EMT gene sets (including associated cZ scores as measure of gene set overdispersion) and by expression magnitude of spheroid phenotype-specific markers VIM and KRT15. **(d)** Violin plots showing expression of individual genes (VIM and KRT15) per identified phenotype-specific clusters for scRNA-seq and full-length pheno-seq. Expression magnitude is plotted as Fragments per Million (FPM, $\log_{10}$). Violin-plot center-line: median; box limits: first and third quartile; whiskers: ±1.5 IQR. **(e)** Boxplots showing expression of individual genes (VIM and KRT15) per phenotype-specific clusters for synthetic pheno-seq profiles. Expression magnitude is plotted as Fragments per Million (FPM, $\log_{10}$) of four independent randomizations. Boxplot center-line: median; box limits: first and third quartile; whiskers: ±1.5 IQR.

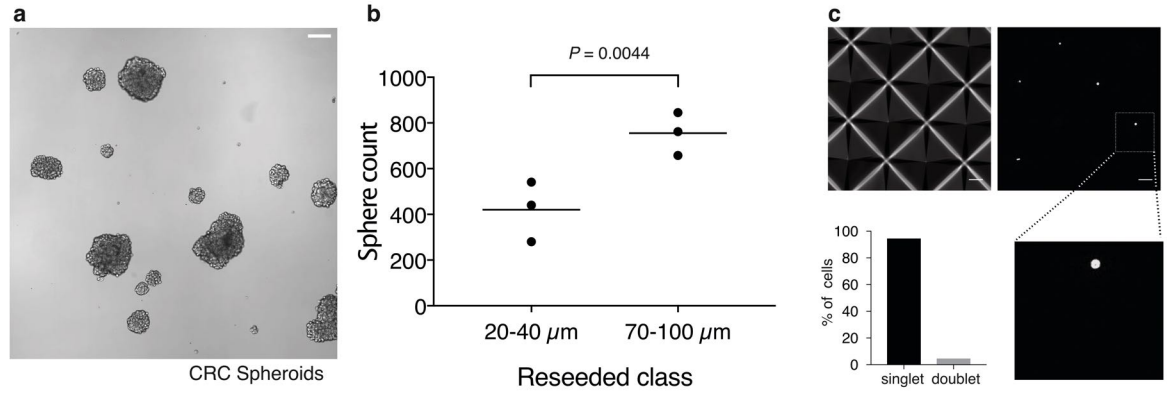


**Supplementary Figure 8 | Experimental basis for pheno-seq of a CRC 3D model (a)** Brightfield microscopy image of reseeded and 10 day cultured clonal CRC spheroids derived from a liver metastasis (scale bar 100 µm, example image of class 70-100 µm in (b)). (b) Reseeding assay with cells isolated from distinct spheroid size classes (20-40 µm and >70-100 µm). Plotted are spheroid counts 10 days after reseeding (three replicates, center-line: mean; indicated P-value of paired two-tailed Students t-test). (c) Single-cell seeding efficiency in inverse pyramidal shaped microwells (upper left) assessed by image analysis. Upper right: Example image of CellTracker Red stained cells seeded in microwells (scale bar: 100 µm). Lower right: Magnified image that corresponds to dashed box in upper right image. Lower left: Quantified cell singlets and multiplets after seeding (three wells, four images per well, 70 objects in total).

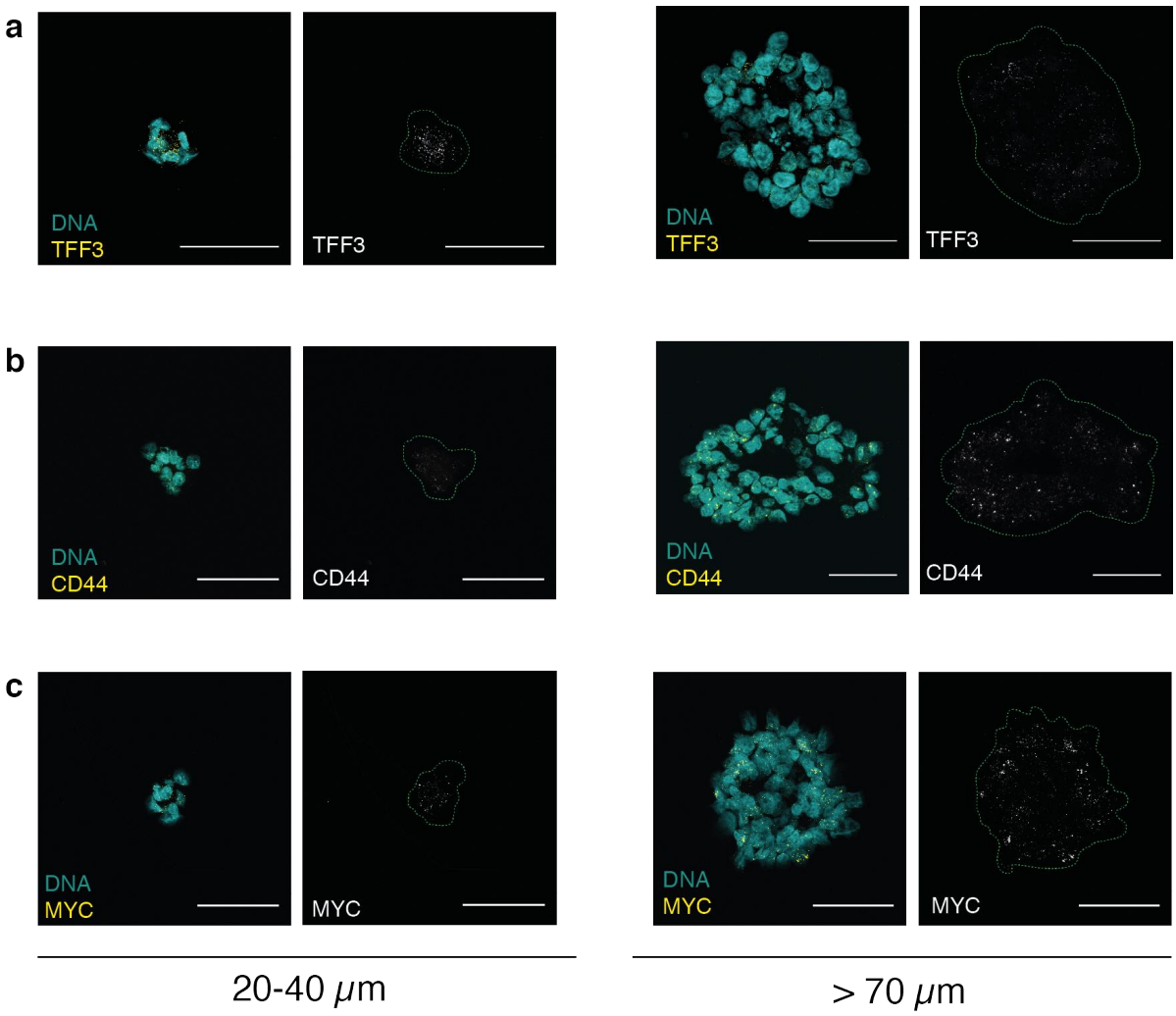


**Supplementary Figure 9 | Validation of CRC pheno-seq data by RNA-FISH (a, b, c)** RNA-FISH example images of different spheroid size classes for differentiation marker TFF3 (a) and cancer stem cell markers CD44 (b) and MYC. (c) Z-projections for RNA-FISH staining of big (>70 µm) and small (20-40 µm) spheroids with (left) and without (right) Hoechst counterstain visualization (Hoechst: cyan; RNA: yellow). Dashed line in images without Hoechst visualization represents spheroid border (scale bar 50 µm).

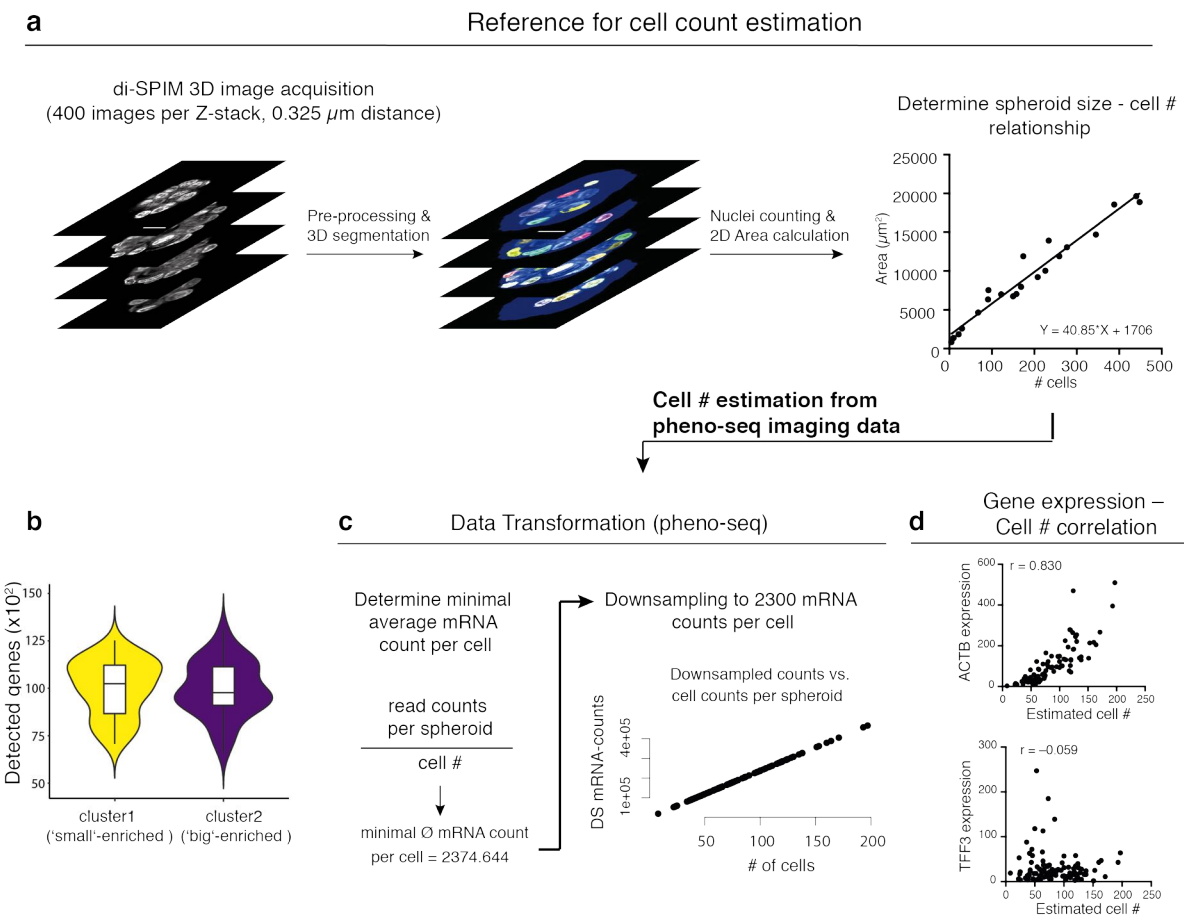


**Supplementary Figure 10 | Estimation of cell numbers from pheno-seq data using a high-resolution reference dataset for data transformation (a)** A two color (Hoechst and CellTracker Red) high-resolution 3D image reference dataset (20 spheroids) is generated by using dual-view inverted selective plane microscopy (di-SPIM). 3D Segmentation and image analysis enables counting of nuclei and the calculated cell number – spheroid size relationship is used to estimate cell numbers from pheno-seq data. **(b)** Violin plots showing detected genes in CRC pheno-seq data per identified cluster. **(c)** Correcting for lost correlation of cell numbers and library complexity by approximating total mRNA abundances in spheroids of different sizes. Raw mRNA counts are divided by estimated cell numbers and the calculated minimal average mRNA count is used to transform the data by downsampling counts to 2300 counts per cell in the whole CRC pheno-seq dataset. Scatter plot showing relationship of estimated cell number and mRNA counts after data transformation. **(d)** Relations of estimated cell numbers and downsampled mRNA counts visualized as scatter plots as well as associated Pearson's correlation coefficients (r) for housekeeping gene ACTB and differentiation markers TFF3.

**Supplementary table 1 | Dataset overview and sequencing information**

| 3D-culture model | MCF10CA | MCF10CA | MCF10CA | MCF10CA | MCF10CA | CRC spheroid |
|---|---|---|---|---|---|---|
| Method | scRNA-seq | Synthetic pheno-seq | Full-length pheno-seq | HT-pheno-seq (control) | HT-pheno-seq (DSP) | HT-pheno-seq |
| Library structure | Full-length C1 | Full-length C1 | Full-length Tube-based | 3`-end iCELL8 | 3`-end iCELL8 | 3`-end iCELL8 |
| Number of samples after library QC | 166 | 8 | 8 | 64 | 210 | 95 |
| Mean total read count per sample | 3,820,057 | 3,685,536 | 9,965,986 | 485,975 | 803,669 | 1,304,480 |
| Mean detected genes (> 0) per sample (all reads) | 8,844 | 15,783 | 12,360 | 8,458 | 8,221 | 9,891 |
| Mean detected genes (> 0) per sample (down-sampled to 100k reads) | 5,554 | 13,374 | 8,411 | 7,051 | 6,377 | 7,412 |

(HT-pheno-seq: high-throughput pheno-seq; control: bottom control with default chip and imaging settings; DSP: Fixation with dithio-bis(succinimidyl propionate crosslinker; C1: Fluidigm C1)

## Supplementary methods

### Assessing single-cell seeding efficiency

Wells with Hoechst 33258 (1 µg/ml) and CellTracker Red CMPTX (10 µM)-stained single-cells wells were imaged with a 10x/0.30 air objective (Leica HC PL FLUOTAR) of a confocal laser-scanning microscope (Leica SP8) one hour after seeding. MCF10CA (24-well) and colon tumor cell (6-well AggreWell400) images (three independent wells) were analyzed with custom made KNIME image analysis workflows to count seeded cell singlet and doublets.

For quantification of single cell seeding efficiency in both MCF10CA and CRC cultutres, cells were segmented based on the CellTracker signal. First, images were flattened by Gaussian convolution (sigma=1), followed by global thresholding using otsu's method. Furthermore, a water shedding (default as implemented in Image J) and a minimum filter (min=5 pixels) were applied and cells touching the border were excluded from further analysis. The same workflow was applied to a duplicated set of images, however radially increasing the size of the labels (Max filter node, span 6) after thresholding, resulting in enlarged cell masks. The generated labels were projected on the previously generated original single-cell segmentations.

### Reseeding assay MCF10CA and 'ilastic' classification

Images were acquired on a Zeiss LSM780 Axio Observer confocal microscope equipped with a 10x/0.3 air objective (Zeiss EC PLAN-NEOFLUAR) in brightfield. For quantification of 'round' and 'aberrant' phenotypes in MCF10CA 3D-cultures we used the random-forest based machine learning software ilastik[49]. A training dataset for the 'Pixel classification' option was first generated on randomly seeded and cultured spheroids, whereas classification was based on images derived from independently reseeded cells from round and aberrant 3D phenotypes. Classification was performed in a custom KNIME workflow by applying the trained model to each image. For quantification of 'round' and 'aberrant' phenotypes in MCF10CA 3D-cultures, spheroids and background pixel classes were first labeled with the paintbrush tool and classified as 'round' and 'aberrant'. Iterative training allowed stable probability maps that distinguished the three object types ('round', 'aberrant', 'background'). For automated analysis of MCF10CA reseeding assays, a custom KNIME workflow loaded a previously trained project file using the 'ilastik headless node'. Images to be classified were imported into KNIME and classified by applying the trained model to

each image. Probability maps for ‘round’ and ‘aberrant’ spheroids were smoothed (manual threshold of 0.5) and a size threshold of 3000 pixels was applied for all segmented objects based on the probability maps. Objects of both classes were automatically counted and assigned to their respective experiment and condition.

**Reseeding assay CRC spheroids**

Images were acquired on a Zeiss LSM780 Axio Observer confocal microscope equipped with a 10x/0.3 air objective (Zeiss EC PLAN-NEOFLUAR) in brightfield. For reseeded colon tumor cells derived from defined size classes ´big´ (70-100 µm) and ´small´ (20-40 µm), 8x8 images per well of the grown spheroids were automatically acquired in 6-well plates (Greiner) using a custom Zeiss VBA macro. All images were analyzed using a custom KNIME workflow to measure spheroid counts per condition.
For quantification of spheroid counts after reseeding of different size classes, spheroid edges were detected using the default function “Find Edges” as implemented in ImageJ. Subsequently, images were manually thresholded (value=20) and neighboring spheroids were separated by applying the default watershedding algorithm to each image as implemented in ImageJ. After segmentation, only segments within the range of 500 to $1x10^5$ pixels (1pix = 0.73 µm) were used and counted for further analysis to exclude single-cells and potential large clusters of spheroids.

**HT-pheno-seq microscopy workflow, image pre-processing and analysis**

For imaging of the iCELL8™ nanowell chip, we used an inverted Leica SP8 confocal microscopy system with an automated stage and the Matrix Screener software extension. In general, also other automated confocal microscopes can be used, but we recommend to use a system where the focus position can be corrected beforehand. A step-by-step microscopy and image analysis protocol can be found in the pheno-seq github repository: https://github.com/eilslabs/pheno-seq.
After spheroids have been dispensed into the iCELL8 chip (see Methods), the tightly sealed chip with spheroids centrifuged upside-down to the foil is fixed on a metallic Chip Spinner (TakaraBio) with adhesive tape and placed into a standard microscope plate holder. At this step, it is important to keep the chip upside-down and to keep the orientation of chip consistent for image processing and analysis. Next, a pre-defined 72x72 grid is loaded and the 4 wells at the upper left corner are used for manual

focusing and adjusting the position (10x/0.30 air objective Leica HC PL FLUOTAR, 0.9x digital zoom). The ´predictive focus´ option was used to extrapolate the correct focus position for the whole chip. At this step, we recommend to control the focus plane for several positions. In addition, the camera orientation of the used microscope should be also checked beforehand. Excitation was set to 405 and 552 nm and emission filter were set to receive signals between 415 – 485 nm (Hoechst) and 555 – 625 nm (CellTracker Red), respectively. Laser intensity and gain were adapted for every experiment, but the pinhole was set to 5.0 Airy Units permanently. One image contained 512x512 pixels, with 2.53 µm pixel size.

For processing of acquired HT-pheno-seq images, we developed an automated image processing pipeline base don KNIME/ImageJ (see github repository: https://github.com/eilslabs/pheno-seq). The two first nodes ("List files") need to be set to the path that contains the locally saved microscopy data on your computer. The workflow is run until the first node after the second metanode named "crop wells and get correct names" (If the the metanode throws an error, the manual parameter for the global threshold needs to be adjusted). Image names were first transformed so that the order generally matches well locations for barcode assignments as the order of image acquisition deviates from default imaging in the standard system. The resulting output was comparable to the output generated by the standard iCELL8 microscope, although with 2x2 wells per field of view instead of 6x6. In addition, images were rotated by 90º to correct for camera orientation of the Leica SP8 system. Subsequently images were cropped to obtain images containing only one well per image instead of four wells in one field of view. For cropping, a mask was built for each well based on the segmentation of the field of view containing the four most round segments over all positions. Since the microscope can image 4 wells in a manner that only minimal offset between well positioning appeared, this straightforward method allowed cropping of all wells over all positions. In the next step, names of cropped images with single wells were transformed to row/column positions for compatibility with iCELL8-specific barcode assignments. For instance, the four wells of the first top-left image (after re-ordering) were transformed to '0_0', '0_1', '1_0' and '1_1'. Further segmentation and analyses were only performed on the cytoplasmic signal (CellTracker Red). The image was first smoothed with a Gaussian convolution algorithm (sigma=5) and then manually thresholded (value=20). Spheroids in close proximity to each other were separated with a

watershed algorithm (ImageJ command ‘watershed’, default parameters). Only segments between 25 and 40,000 pixels were considered for further analysis to exclude artefacts and single-cells. Segments touching the border of the image were excluded. Cropped well images were saved automatically in designated locations individually for each channel but also as overlay of the two channels for better visualization in the Shiny app. The images are then converted to .png format using a custom ImageJ macro. In the last step, a .csv file was generated that contained names of all wells containing at least one spheroid. Additionally, calculated 2D features (derived from KNIME image processing node ‘Feature Calculator’) of the corresponding labels were appended (e.g. size and circularity).

The saved .csv file containing spheroid statistics was automatically handled by a custom R script and embedded together with the images in an interactive R/shiny application (PhenoSelect). This allows manual browsing through the acquired images and visualization of spheroids together with their respective image feature statistics. Moreover, the application allowed for visual inspection of the given image features over the whole population, allowing the identification of specific subtypes, e.g. by a particular shape or size. To characterize absolute spheroid sizes, the respective major axis length value (in pixels) was multiplied with the physical length of a pixel in the segmented object. Subtypes of spheroids can be selected by applying different sets of thresholds (e.g. size, circularity) and individual wells can be discarded if necessary (e.g. due to imaging artefacts). The list of selected wells can be saved at any time and also reloaded to proceed with selection at a later time-point. Furthermore, comments can be added to individual wells. Control wells can be selected individually. Once the desired number of wells to be sequenced had been selected, the application generated the ‘filter file’, which is then used to program the iCELL8 dispenser software. In addition, a ´well-list file´ was generated that contained well-barcode assignments for demultiplexing as well as calculated image features for selected spheroids. Finally, we implemented plotting of image features on pre-computed t-SNE maps based on gene expression generated by PAGODA (see below). After sequencing of selected spheroids, this tab enabled integrative analysis for direct association of functional visual phenotypes to transcriptomic heterogeneity.

**Leakage test**

Due to the additional centrifugation step to the foil, we assessed potential leakage by dispensing a highly fluorescent solution of PBS + 1 µg/ml fluorescein sodium salt (Sigma) into one half of the nanowells and dispensed only PBS into the other half and into control wells. A dispensing pattern was chosen to generate a maximum number of borders between nanowells filled with fluorescein and those only filled with PBS. Subsequently, the chip was processed and imaged as described above but with laser and filter sets matching the fluorescent properties of fluorescein ($\lambda_{ex}$ 460 nm; $\lambda_{em}$ 515 nm).

The acquired images were processed for well assignment, segmentation and cropping by the HT-pheno-seq pre-processing workflow and average fluorescence intensity was measured for every well independently. Average fluorescence intensity values ranging from 0 to 255 (8 bit) were color coded and plotted onto a 72x72 grid resembling the iCELL8 chip layout using a custom R script.

**Cell count determination by light sheet imaging and 3D segmentation**

To estimate the cell number in spheroids in HT-pheno-seq experiments based on acquired images, we generated a high-resolution 3D reference dataset to determine the linear relationship of size (area) and cell count. CRC spheroids were stained with 1 µg/ml Hoechst and CellTracker Red CMPTX (10 µM) for 3 hours and isolated and fixed as described above. Subsequently, spheroids were mounted in 2% low-melting agarose (Sigma) and 3D images were acquired using a Dual-View Inverted Selective Plane Illumination Microscope (ASI di-SPIM) using Nikon 40x/0.80W NA NIR-Apo water dipping objectives. Dual view raw data was processed to generate isotropic images at a resolution of 0.325px/µm (400 images per Z-stack, 0.325 µm distance). Pre-processing and 3D segmentation were performed with a custom KNIME workflow. To count nuclei from the high-resolution light sheet microscopy dataset, a 2D projection of the smoothed CellTracker image produced a mask that was generated individually for each spheroid. The obtained 2D mask covering the spheroid was applied to all individual slices, in order to count nuclei only within this area to exclude artifacts. Single-cells were first segmented and counted individually for each slice. Subsequently, overlapping cells were separated by a watershed algorithm (KNIME node: Waehlby Cell Clump Splitter). Furthermore, the 2D segmentations were used as ‘seeds’ for three-dimensional Voronoi segmentation, in

order to obtain a three-dimensional segmentation that accounts for cells spanning multiple slices. Cell counts (without correction for potential changes in ploidy) and corresponding 2D spheroid dimensions were exported from KNIME and further analyzed and plotted using a custom R script. Briefly, we first converted the respective pixel numbers for minor and major axis of all 2D spheroid masks to metric distances. Facing the challenge of variable spheroid morphologies, we further approximated the spheroid size as the product of its biggest and smallest diameter (i.e. the minor and major axis). Subsequently, we plotted the approximated size of every spheroid against its respective cell count determined by 3D segmentation in KNIME. A linear model was fitted through the points and the obtained slope was used to calculate cell number estimations for HT-pheno-seq experiments.